Polymer Testing 102 (2021) 107311

Contents lists available at ScienceDirect

Polymer Testing

journal homepage: www.elsevier.com/locate/polytest

# The experimental and numerical analysis of the ballistic performance of elastomer matrix Kevlar composites

S. Samaneh Asemani [a], Gholamhossein Liaghat [a,b,*], Hamed Ahmadi [a], Yavar Anani [a], Amin Khodadadi [a], Sahand Chitsaz Charandabi [c]

[a] Department of Mechanical Engineering, Tarbiat Modares University, Tehran, Iran
[b] School of Mechanical &Aerospace Engineering, Kingston University, London, England, United Kingdom
[c] School of Mechanical Engineering, Coventry University, England, United Kingdom

ARTICLE INFO

*Keywords:*
Numerical analysis
High-velocity impact
Failure mechanism
Elastomeric composite

ABSTRACT

In this paper, the behavior of high-velocity impact of Kevlar fabric and elastomer composites was investigated both experimentally and numerically. The experimental tests were performed by a gas gun device and hemispherical projectiles at different velocities, ranging from 122 m/s to 152 m/s for 2- and 4-layer samples. The penetration resistance of these composites during impact was determined using ABAQUS/Explicit. The present study's novelty lies in choosing the finite element model for Kevlar fabric and elastomer matrix in composites with nonlinear behavior to estimate the damage mechanism in the impact zone. For this purpose, the material model of the formable was used to define the damage criteria for Kevlar, and the material model of the VUMAT was used to consider the non-linear behavior and damage evolution of elastomer matrix with one of the damage criteria. Then, the dynamic behavior of the laminate was studied by a Split Hopkinson Pressure Bar. The effect of the number of layers, the shape of the projectile, the energy absorption and failure mechanisms were studied. The verification of this numerical model with experimental observations showed good agreement. The results reveal that elastomeric composites can cause to increase energy absorption and reduce the damaged area.

## 1. Introduction

One of the most critical issues in mechanical engineering is structures that are exposed to impact loads of such substances as metal or composite. Today, in many engineering applications with advanced technology, composites are known as the best choice for many passenger, combat, vehicle, and military uses [1–4]. The need for materials with a high stiffness-to-weight ratio and high strength-to-weight ratio has led to the rise of composites. Despite these general features, however, composites are fragile and susceptible to damage from a number of sources, both during initial processing and in service. Even seemingly minor impact events can greatly damage a thin-walled composite structure [5]. Thus, it is crucial to study into the mechanical properties and failure mechanisms of elastomeric composite under different velocities for the assessment of elastomeric composite after impact. Considering the substantial efforts required to carry out experimental tests, it is important to progress reliable and efficient numerical methods to predict the response of elastomeric composite structures under different velocities. For this reason, some comprehensive studies on the failure mechanisms of a large variety of composite laminates structures by numerical methods can be found in Refs. [6–8]. In order to comprehensively study the impact phenomena, key influence factors such as impact energy, impact location, impact shape and thickness of the face plate and their materials have also been considered. Researchers are increasingly interested in giving energy absorbing devices a higher capacity to protect their occupants from injury. Thin-walled structures have been extensively used as energy absorbing devices; and ongoing efforts over the past few decades have been devoted to investigating the energy absorption capacity of a range of structural configurations made of various metals under dynamic impact condition using finite element analysis [9–15]. An additional analytical methodology for determining on the energy balance in the development of damage on impact with the help of a localized strain field was introduced in Ref. [16]. Nevertheless, analytical approaches, which can be adopted for only a few specific conditions [17–19], mostly cannot be considered for a complete and meticulous study of impact events, due to the intrinsic complexity of

* Corresponding author. Department of Mechanical Engineering, Tarbiat Modares University, Tehran, Iran.
*E-mail addresses:* Ghlia530@modares.ac.ir, G.Liaghat@kingston.ac.uk (G. Liaghat).

https://doi.org/10.1016/j.polymertesting.2021.107311
Received 3 April 2021; Received in revised form 17 July 2021; Accepted 1 August 2021
Available online 5 August 2021

impact behavior itself [20–22]. The finite element method (FEM) is the most common method used for failure mechanisms and damage tolerance studies among all the numerical approaches [23,24]. A more widespread study of impact behavior can be more accurately achieved by numerical methods. Indeed, finite element method codes can be implemented to model impact events on a composite specimen, taking into account both intra- and inter-laminar damages [25–27]. Against this background, it is hard to find studies related to aramid fiber-reinforced composites. The material model composite was used to simulate high-velocity impact on a combat helmet manufactured from aramid fiber-reinforced composites, and several studies can be found in the literature where the material model composite was implemented for modeling glass fiber-reinforced composites. Also, damage evolution and penetration of thick-section composites were studied using explicit finite element model (FEM). The finite element analysis included initiation and advanced damage of the composite during impact [28–33]. In Ref. [34] experimental tests were carried out to investigate the effects of certain composite features (like multilayer structure), the geometry of projectiles, the velocity of impact and the influence of boundary conditions (constraints) on the test responses. The effects of contact force models on the global and local dynamics of a drifting multivibrator were worked by in Refs. [35,36]. The non-linear analysis of the considered system indicated that the local and global dynamic behaviour depended on the choice of the contact force model.

The impact response of fiber-reinforced polymer matrix composite is studied by Andrew et al. [37]. The structural behavior of composite and the influence of impact velocity on different failure modes were discussed to determine the impact resistance. Pach et al. [38] studied the experimental and numerical analysis of the ballistic resistance of polymer composites. They presented the analysis of failure caused by a ballistic impact, further compared to the results of computer simulations conducted using the finite element method (FEM). Moallemzadeh et al. [39] worked on morphological and mechanical behaviors of polymer composite plates reinforced with surface modified glass fiber woven under high-velocity impact in term of energy absorption of the plates. Morphological studies were conducted by SEM analysis. Taherzadeh et al. [40] investigated the effect of an elastomer layer into conventional fiber metal laminates on their perforation resistance. Numerical simulation of the penetration process was performed using the advanced finite element code. It could be found that adding an elastomeric layer into the structure was more useful than composite thickening at the same thickness in terms of improving energy absorption efficiency. The numerical and experimental results in the study of composite armour systems consisted of ceramic and ceramic-elastomer composites for ballistic protection was investigated by Chabera et al. [41]. The modeling of protective structures was performed by the finite elements method. The residual energy and crack propagation by intermediate composite layer was tested and analyzed. The behavior of rubber, as an incompressible hyperelastic material, was modeled [42]. Pouriayevali et al. [43] studied the large deformation response of incompressible elastomeric materials at high strain rates. Ahmad et al. [44] worked on the ballistic impact resistance of high-performance fabrics and the energy absorption of coated with natural rubber under impact loading. The ballistic limit performances and energy absorption of the fabric systems were compared with unstitched fabric system. Higher ballistic limit and higher energy absorption with the system containing fabric layers coated by natural rubber achieved than the all-neat layer fabric system. New two-dimensional wake oscillator model of flexible structure was proposed [45]. High flexibility of rubber jointed with high strength fabric form an impact resistance composite suitable for ballistic impact and penetration resistance [46]. Roland et al. [47] worked on elastomer–steel composite laminate armor to increase the penetration resistance. Sarlin et al. [48] studied the performance of steel/rubber/composite plates and determined that the use of rubber could reduce the damaged area by 50%. This damaged area was shown to increase proportionally with the impact energy. Stoll et al. [49] experimentally and numerically studied the influential damping of factors and the mechanical properties of this laminate and observed the dependency of natural frequencies in various modes and the flexural stiffness of the elastomer thickness. The strain rate dependent in-plane and the through-thickness deformation and failure behavior of textile reinforced polypropylene were investigated [50]. Khodadadi et al. [51] investigated the impact performance behavior of hyperelastic rubber panels and determined that higher amounts of elastomer hardness could lead to better impact resistance. The high-velocity impact response of carbon fiber reinforced polymer was tested and analyzed [52]. Bandaru et al. [53] studied the role of fabric architecture and ballistic impact response of Kevlar reinforced thermoplastic composite armors. The damage patterns achieved from the simulations were compared with the experimental results to evaluate the performance of the simulations. An efficient simple numerical method, known as energy-based collocation, evaluated the nonlinear behavior of a geometrically imperfect composite plate. Plates with different boundary conditions and different thickness were considered. The analysis was performed by a computer program developed based on FORTRAN language [54]. A numerical and experimental study of the failure and ultimate strength of composite plates under in-plane and lateral pressure was conducted by Ghannadpour et al. [55]. They used Hashin failure criteria to predict the failure location and the corresponding material properties of the failed zone.

In the present study, the high velocity penetration behavior of Kevlar/elastomer composites is experimentally and numerically investigated. It is easy to develop a reliable geometrical model to simulate real linear behavior structures. But one of the difficulties in modeling elastomeric composites is the failure of their behavioral model, due to their nonlinear behavior. The purpose of studying a structure in this context is to learn about the dynamic behavior of composite structures during the ballistic impact and also to investigate the increase of energy absorption, which has not been evaluated in previous studies. Specimens were evaluated in terms of damage mechanisms and impact resistance. The commercially available 3D dynamic nonlinear software, ABAQUS, with user-defined material models (VUMAT), was used to simulate the dynamic behavior of the specimens. A numerical parametric study energy absorption of the composite under impact load was made, paying attention to the effect of the number of layers of the damaged composite, the effect of strain-rate on the composite and the impact of the shape of the projectile at different velocities on the ballistic performance. This paper is divided into sections. In Section 2 the ballistic experimental tests are presented with a description of the gas-gun and split Hopkinson pressure bar (SHPB) device used for the tests, together with the features of the targets and the projectile. In Sections 3 and 4 the creation of numerical models is described in detail step by step. In Section 5 the results of the numerical models and experimental tests are critically compared in order to validate the numerical methodology; finally, the residual velocity and energy absorption, analysis are reported. In Section 6 the different projectile shapes are described. In Section 7, finally, the results from the numerical models are used for further investigation of the limits of ballistic velocity and damage mechanism analysis of composites.

## 2. Experimental method

### 2.1. Materials and fabrication

The fabric and the matrix used in the high-velocity impact tests were Kevlar fabric and natural rubber. A natural rubber matrix underwent the process of vulcanization, which is a chemical process for converting raw natural rubber into a substance with desired properties by the addition of fillers, activators, sulfur or other equivalent curatives and accelerators. These additives modify the rubber by creating cross-links between polymer chains. In this study, the HH type of rubber was used to ascertain the impact resistance of rubber matrix composites. The NR compound formulation for the HH type of rubber compound is presented

**Table 1**
Formulation of compounds [56].

| Ingredients | | Loading (Phr) |
|---|---|---|
| | Supplying company | High Hardness |
| NR (SMR 20) | The Rubber Research Institute,Malaysia | 100 |
| Carbon Black (N330) | Pars, Iran | 60 |
| Zinc oxide | LG, Korea | 5 |
| Calcium carbonate | Yazd Tire, Iran | 30 |
| Spindle oil | – | 15 |
| Sulfur | LG, Korea | 2 |
| Volcacit | – | 0.7 |

in Table 1. In this study the HH type of rubber compounding was carried out in an open two-roll mixing mill (Polymix 200 L, Germany) at 40 rpm with a mixing time of 15 min. An Oscillating Disc Rheometer (ODR) model 4308 (Zwick Co., Germany) at 160 °C determined the vulcanization characteristics of the NR compound. A disc was embedded in the test piece and oscillated through a small specified rotary amplitude to the cure characteristics of the rubber compound [56]. The cure characteristics of a rubber compound are presented in Table 2. In this table, $t_i$ indicates the time required for i% of torque increases.

The impregnation of the Kevlar fabric in preparing the rubber matrix composite target was facilitated by diluting the rubber compound in Toluene at a 2:3 vol ratio. Individual fabric layers were soaked in the diluted rubber compound for 24 h. After impregnation with the toluene/rubber mixture, the fabric layers were left in an ambient temperature for 24 h and then put in an oven at 40 °C for 2 h to remove the toluene. Then 2 and 4 coated fabric layers were assembled and subsequently cured under hydraulic pressure at 160 °C by a 25ton hydraulic press based on rheometer results [56].

### 2.2. Impact test

The ballistic impact behavior of a Kevlar/elastomer composite target of different thicknesses against a hemispherical projectile was studied. The experimental mechanical properties were provided in the Impact Lab. of Tarbiat Modares University [56]. The same set of properties were used for the numerical model presented. The incident ballistic impact

**Table 2**
Curing characteristics [56].

| | $t_5$ (min) | $t_{10}$ (min) | $t_{90}$ (min) | $t_{95}$ (min) | $t_{100}$ (min) | Lowest torque in the vulcanization process $M_{max}$ (lbf.in) | Highest torque in the vulcanization process $M_{max}$ (lbf.in) |
|---|---|---|---|---|---|---|---|
| HH rubber | 0.28 | 0.721 | 2.9 | 3.4 | 5.301 | 7.375 | 101.8 |

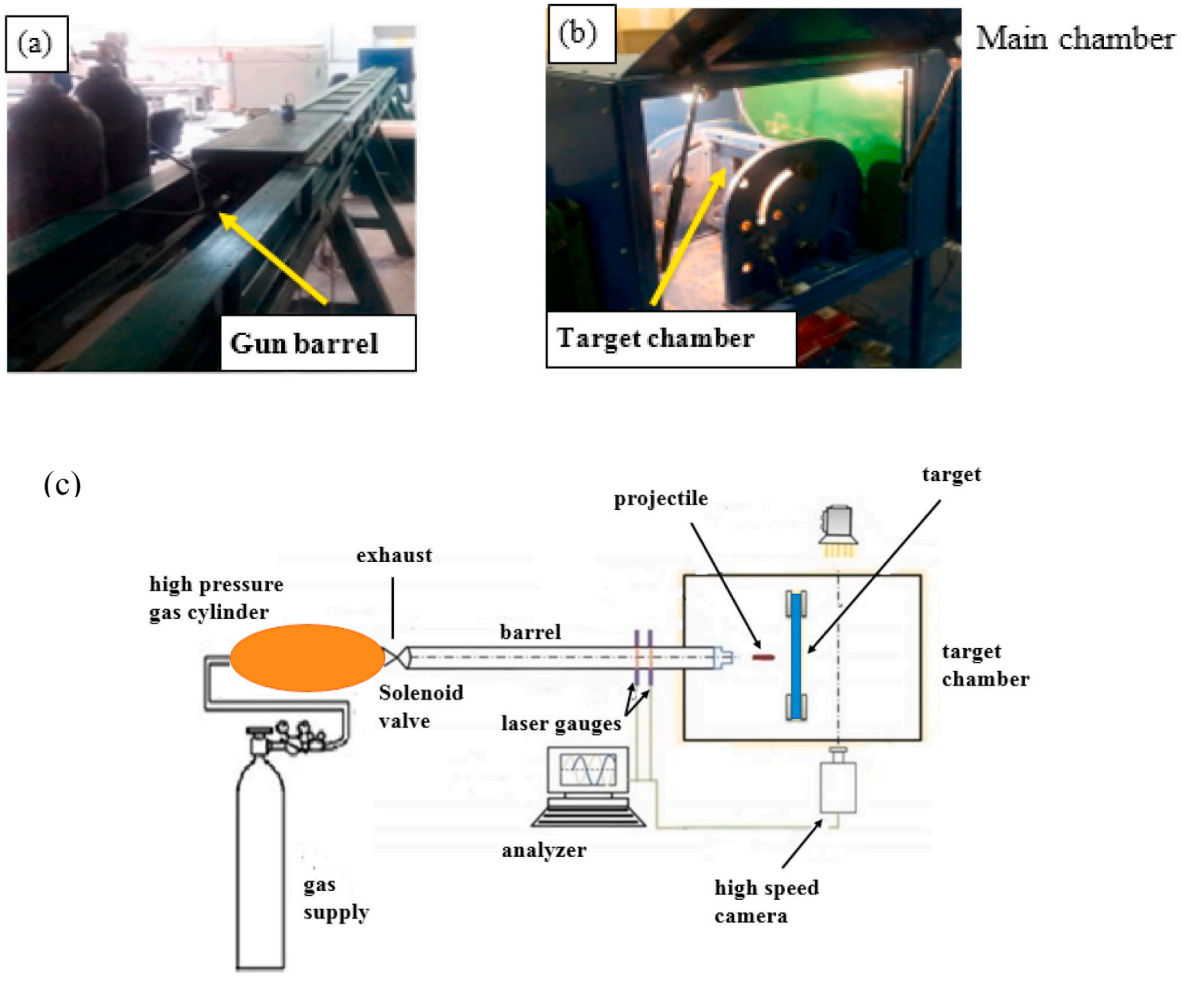


**Fig. 1.** The test of high-velocity impact (a) Gas gun, (b) Main chamber, (c) Schematic of the gas gun device.

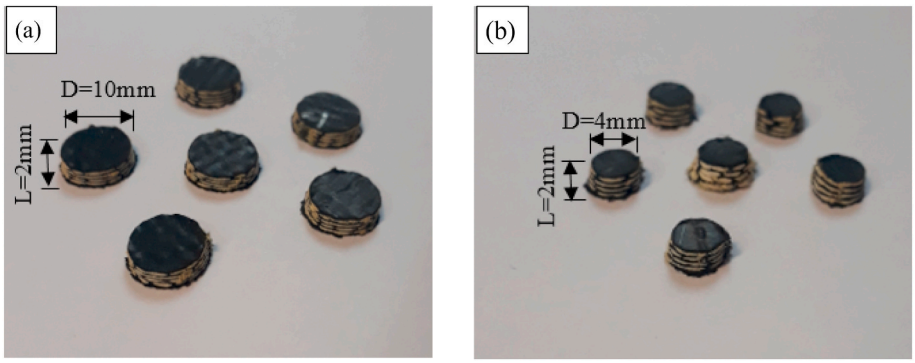


**Fig. 2.** Samples composite: (a) with a diameter of 10 mm (L/D = 1/5), (b) with a diameter of 4 mm (L/D = 1/2). Both sets of images under high-velocity impact.

**Table 3**
Preparation of the elastomers analyzed in the study.

| Sample type | (bar) Pressure | L/D | Strain rate ($S^{-1}$) |
|---|---|---|---|
| Kevlar/elastomer | 7 | 1/2 | 6220 |
| Kevlar/elastomer | 4 | 1/2 | 6093 |
| Kevlar/elastomer | 7 | 1/5 | 6200 |
| Kevlar/elastomer | 4 | 1/5 | 5712 |

was made using the numerical model. The details of the projectile and the target characteristics used for the experimental and numerical model studies are listed below:

Projectile: hemispherical projectile, hardened steel projectile with mass, $m_p = 9.32$ gr; diameter, $d_p = 10$ mm.

Target: fabric Kevlar/elastomer composite, unsupported area of the target 50 × 50 $mm^2$, and thickness 1–2 mm.

Studies of the high-velocity impact were performed using a gas gun on a woven fabric Kevlar/elastomer composite with a velocity range of 117–125 m/s for two-plies, and 143–152 m/s for four-plies. The gas gun was composed of a high-velocity firing valve, a pressure vessel of 120 bar capacity, and a hollow steel barrel 6 m long. The inside diameter of the barrel was 10 mm. The samples were ultimately constrained in the fixture and were set on all four sides of this in the target chamber. The exact impact velocity of the projectile was measured with two laser gauges just before impact on the target; in addition, the residual velocity was recorded by a high speed camera via a shadowing procedure, as presented in Fig. 1. The tests at each velocity on the composite target were carried out three times. The ballistic limit was measured to be the most important outcome of the ballistic test. The ballistic limit velocity, $V_{BL}$ is defined as the incident impact velocity for a specific projectile and target combination, leading to the complete penetration of the target with the projectile tip reaching the back face of the target at zero velocity. It may not be possible to achieve $V_{BL}$ experimentally; for experimental studies, therefore, $V_{50}$ was used instead of $V_{BL}$. $V_{50}$ is defined as the average of the equal number of the highest partial penetration velocities and lowest whole penetration velocities of a specific projectile and target combination that take place within a specified velocity range. A minimum of three parts and three whole penetration velocities are used to compute $V_{50}$ [57]. Hence, the experimental ballistic limit velocity for Kevlar/elastomer composites of 2 and 4 layers were 64 m/s and 122 m/s, respectively.

### 2.3. Split Hopkinson Pressure Bar (SHPB) test

The investigation of the dynamic behavior of materials, especially elastomeric composites under impact loading conditions at high strain rates, is considered an additional reliability factor. In this study, the samples were 4-layer Kevlar/elastomer composites with a thickness of 2 mm and were cut by means of water jet cutting. This process uses only a high-pressure water jet or may add an abrasive medium. The study of strain rate on these composites is performed experimentally only with a Hopkinson pressure bar device in the Mechanical Laboratory of Bu-Ali Sina University. To reduce the side effects during the test, all samples were glued in place. The geometry and dimensions of the samples are shown in Fig. 2. The measurement diameters of the samples were 4 mm and 10 mm and the volumetric percentage of fiber in the composite samples was 46%.

Table 3 shows the different strain rates considered as samples for testing by the Hopkinson pressure bar at different length-to-diameter ratios. To investigate the effects of friction between the incident and transmission bars, and the front and back surfaces of the samples, the coefficient of friction of zero was chosen.

A Hopkinson pressure bar usually involves 3 bars, such as a striker, an incident, and a transmission bar [58–60]. Fig. 3 shows a Hopkinson pressure bar device. Tables 4 and 5 show, respectively, the dimensional and mechanical properties of the device. A stress wave is produced and travels down the incident bar toward the sample. In the Hopkinson test method, the signals including the incident wave $\varepsilon_I$, reflected wave $\varepsilon_R$, and transmitted wave $\varepsilon_T$ are used to calculate the torque, strain, stress, and strain rate in the sample, as follows [60]:

$$\dot{\varepsilon}_s(t) = -(2\,C_0 / l_s)\int_0^t \varepsilon_R(t)\,.\,dt \tag{1}$$

$$\sigma_s(t) = (A_0\,E_0 / A_s)\,\varepsilon_T(t) \tag{2}$$

where $E_0$, $C_0$, $A_0$, $A_s$, and $l_s$ are the Young modulus, elastic wave velocity, the cross-sectional area of the bars, initial cross-sectional area, and initial length of the sample, respectively.

Fig. 4 shows the strain rate-time curves for the Kevlar/elastomer composite sample using the strain obtained from the voltage recorded by the strain gauge and according to equation (1). The stress-strain curves are obtained using equation (1) and the integration of equation (2). It can be seen in these figures that, at the same $L/D$ ratio, the strain rate increases with increasing pressure. Furthermore, Fig. 5 shows the stress-strain curves of the Kevlar/elastomer composite in the direction of thickness at different strain rates and different $L/D$ ratios. These figures suggest that the behavior of the samples depends entirely on the loading rate. Moreover, in dynamic loading at a certain $L/D$ ratio, the amount of stress increases with increasing pressure, which means that incident loading is more effective in improving the compressive strength. Furthermore, the Kevlar/elastomer composite depends on the strain rat; hence, as the strain rate increases, the yield stress, and failure strain increase. However, for thermoset composites [61], the failure strain decreases with the increasing strain rate. It can be seen from these figures that the non-linear behavior affects the stress-strain curves of all the samples. It causes the strain to increase during loading and to reduce the composite failure, while the effect of non-linear behavior is not seen in the stress-strain curves of the thermoset composites [61]. As the strain rate increases, the compressive strength of the samples and the strain on

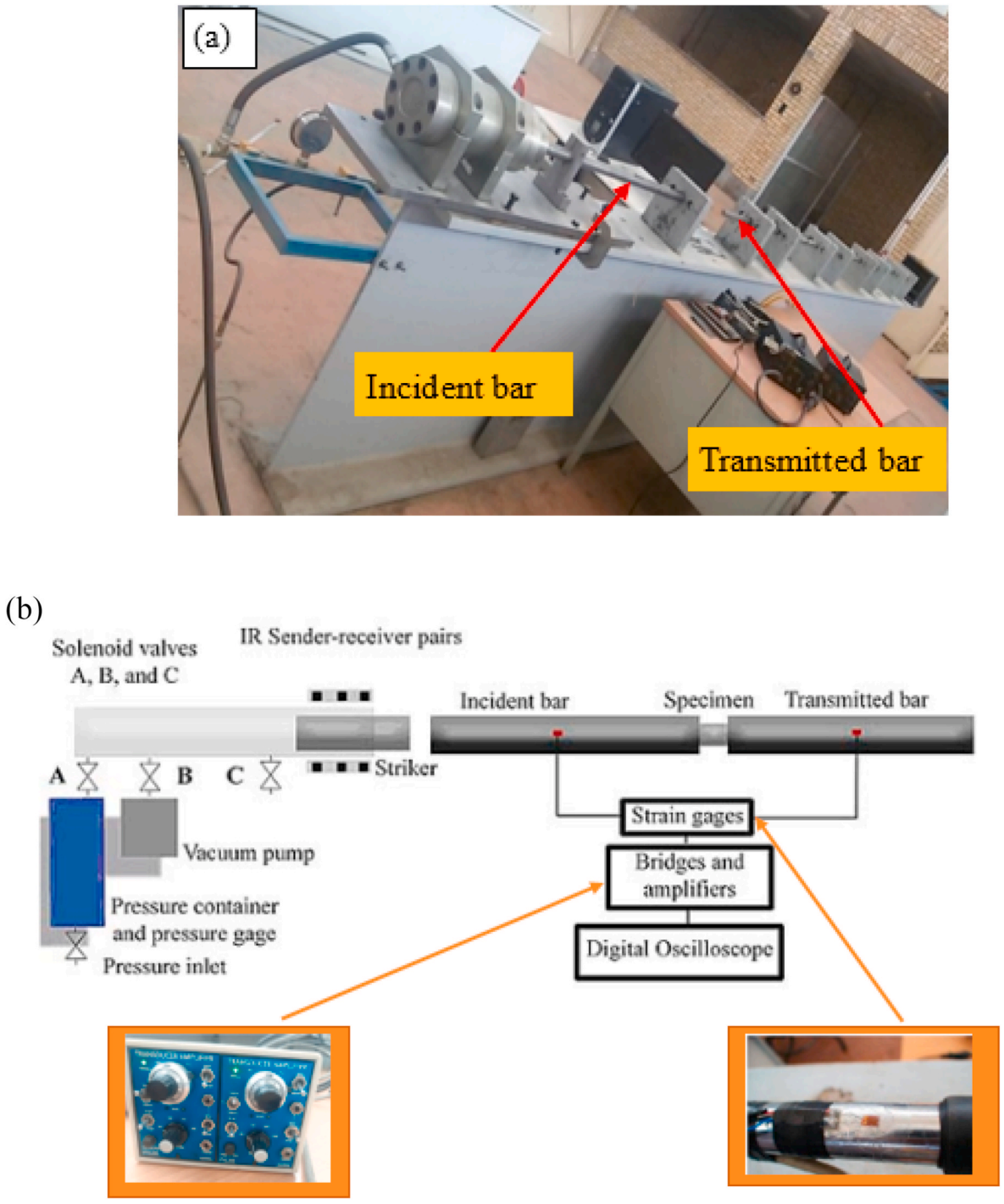


**Fig. 3.** (a) A tensile Hopkinson pressure bar device, (b) Schematic diagram of the Split-Hopkinson Pressure Bar.

**Table 4**
Dimensional specifications of Hopkinson device.

| Dimensions | | | |
|---|---|---|---|
| Material | (cm) Length | (cm) Diameter | |
| Marching Steel | 50 | 2.5 | striking bar |
| Marching Steel | 195.5 | 2.5 | incident bar |
| Marching Steel | 195.5 | 2.5 | transmission bar |

**Table 5**
Mechanical properties of Hopkinson device.

| Samples type | $\rho$( kg/m3 ( | $E$(GPa ( | (m/s) $C_0$ |
|---|---|---|---|
| Marching Steel | 8000 | 200 | 5000 |

the samples increase by more than 80% and 30%, respectively. This is due to the slow movement of the displacements, which ultimately increases the stress required to change the shape of the composite target. Therefore, at low strain rates, the chain moves so fast that it changes the intermolecular structure. In contrast, at high strain rates, as the loading

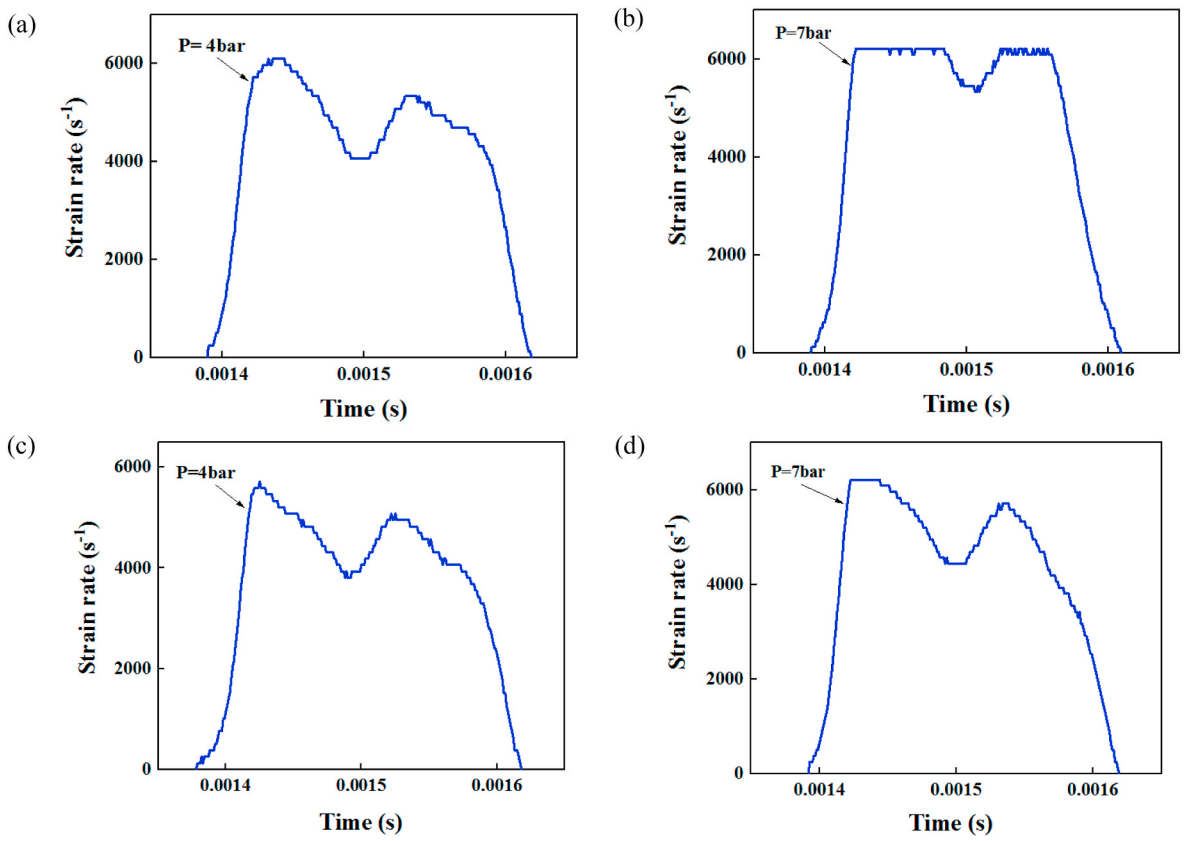


**Fig. 4.** True data from the SHTB experiment for fabric Kevlar/elastomer composite and comparison strain rate – time curves at different initial pressure:(a–b) with D = 4 mm, (c–d) with D = 10 mm.

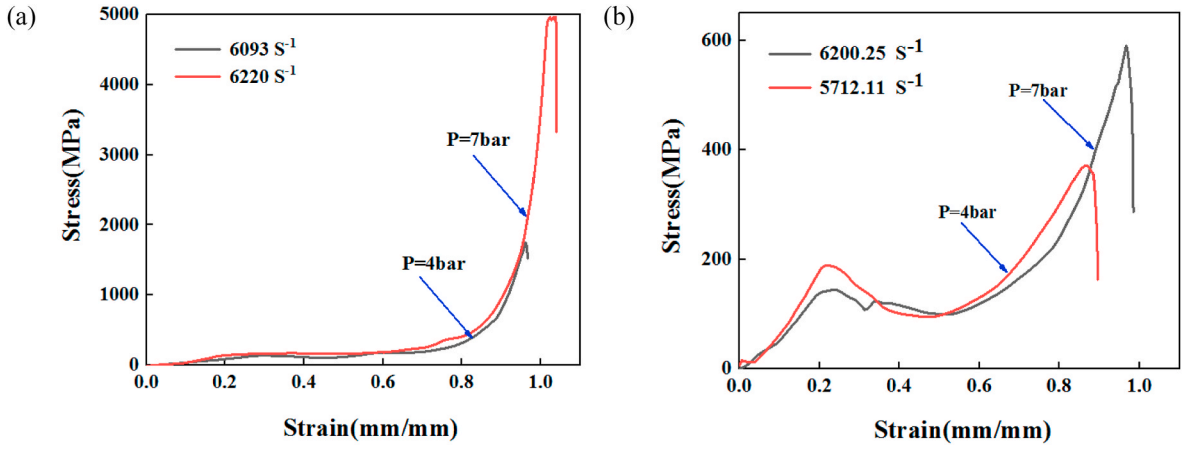


**Fig. 5.** Effect of the strain rate at different initial pressures on the tensile stress–strain plot for fabric Kevlar/elastomer composite: (a) with D = 4 mm, (b) with D = 10 mm.

speed increases, there is not enough time for the transfer of force between the molecular chains in the extensive scale, and there is only a small range of interactions.

## 3. Numerical simulation

### 3.1. Fundamentals of failure model

The strength of a composite structure is a function of the strength of its constituent layers. The process of the failure of composites with homogeneous isotropic materials is different because they are non-isotropic. A variety of stress combinations can cause failure in non-isotropic materials. In examining the failure of composites, the behavior of each layer is investigated. Whenever the stress distribution causes a layer to fail, the calculation of failure proceeds by removing that layer. In general, the study of composite failure has many complexities, for reasons such as layer collapse, fiber failure, fiber buckling, resin failure, cavities and cracks, and so on. To choose the best model, various parameters such as the type of structural loading, collision speed, damage mechanisms, and failure models should be considered.

#### 3.1.1. Matrix failure criterion

One of the ways of studying non-linear elastic materials enduring large deformation focuses on hyperelasticity. Rubber is a good example

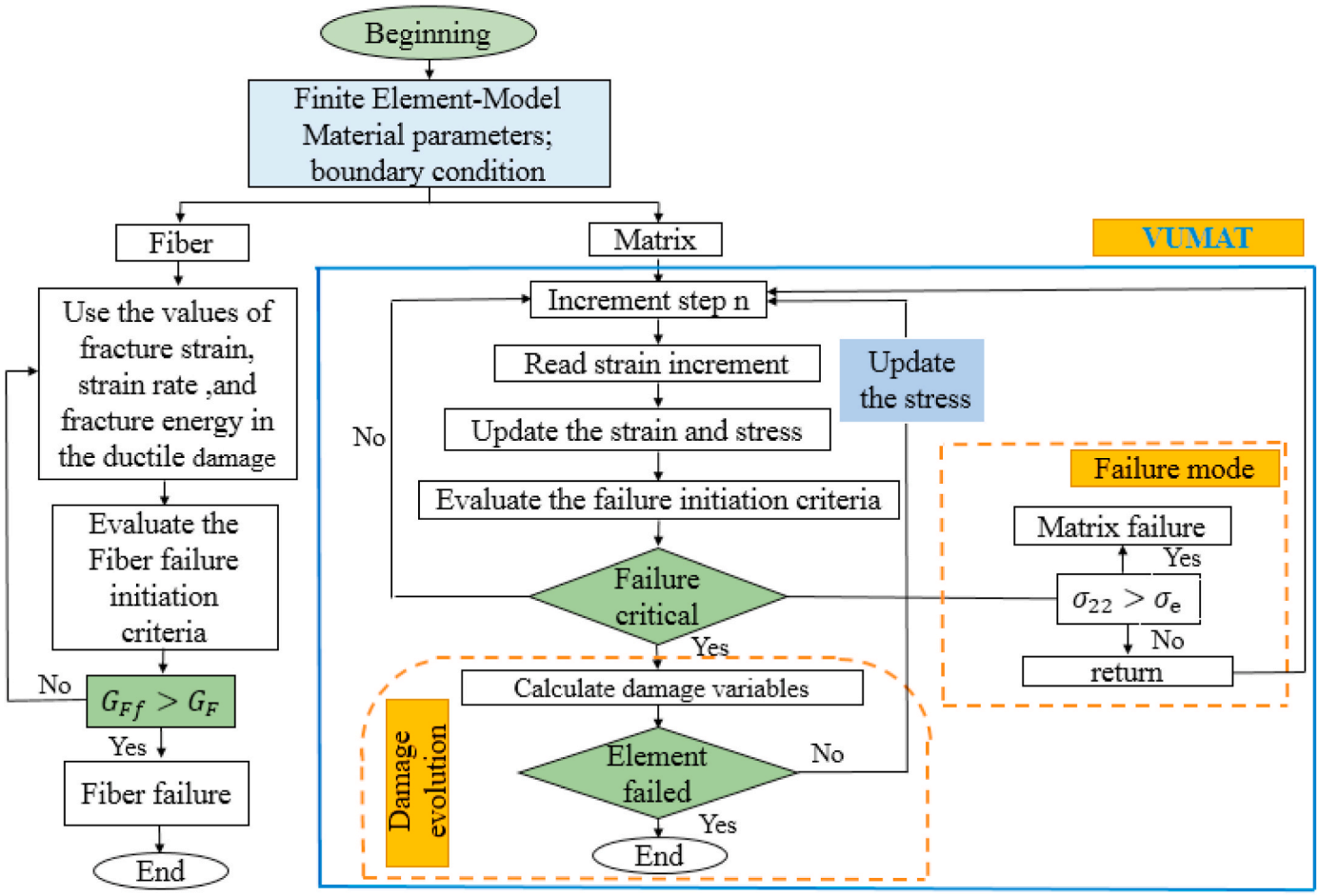


**Fig. 6.** Flow chart depicting the numerical model.

of a hyperelastic material. In hyperelasticity, the stress is not considered directly from the strain unlike linear elastic materials. In general, for isotropic materials (e.g., rubbers), the strain energy function (SEF) can be indicated in terms of right (or left) Cauchy Green tensor $C$ (or $B$) invariants ($I_1$, $I_2$, $I_3$) or eigenvalues of deformation gradient tensor $F$, defined principal stretches ($\lambda_1$,$\lambda_2$,$\lambda_3$). i.e. [62] $W = W(I_1,I_2,I_3)$ *or* $W = W(\lambda_1,\lambda_2,\lambda_3)$. For rubber material, due to the negligible compressibility under conventional pressures, the incompressibility hypothesis is often used$I_3 = 1$. Therefore, we determine that $W = W(I_1, I_2)$. The fundamental relation for materials of hyperelastic is [62]:

$$S = 2\left(\frac{\partial W}{\partial I_1}I + \frac{\partial W}{\partial I_2}(I_1 I - C) + \frac{\partial W}{\partial I_3}I_3 C^{-1}\right) \tag{3}$$

The second Piola-Kirchhoff stress transformation to Cauchy stress tensor $\sigma$ gives [62] $\sigma = 2F(\partial W/\partial C)F^T \rightarrow \sigma = (1/J)FSF^T$ where $J = \det F$. Furthermore, for incompressible materials like rubbers, W are the only function of the first and the second principal invariants of B [62].

$$\sigma = 2\left(\frac{\partial W}{\partial I_1}B + \frac{\partial W}{\partial I_2}(I_1 B - B^2)\right) - pI \tag{4}$$

In which $I$ is the identity tensor, and $p$ is the hydrostatic pressure determined from boundary conditions. In this study, the energy density function is initially assumed by the Neo-Hookean constitutive model, and an incompressible material is given by $W = C_1(I_1 - 3)$ [62] where $C_1$ is a material parameter. In this test, the material is stretched in one direction ($\sigma_{22} = \sigma$) while remaining stress-free in other directions ($\sigma_{11} = \sigma_{33} = 0$). For uniaxial loading conditions, the nonzero Cauchy stress component is:

$$\sigma_{22} = 2C_1\left(\lambda^2 - \frac{1}{\lambda}\right) = 2C_1\left(\frac{3\varepsilon_{22} + 3{\varepsilon_{22}}^2 + {\varepsilon_{22}}^3}{1 + \varepsilon_{22}}\right), \lambda = 1 + \varepsilon_{22} \tag{5}$$

In this part, a user defined subroutine VUMAT in ABAQUS/Explicit with FORTRAN code was employed to simulate the progressive failure and damage evolution of an elastomer matrix material of composite laminates. The stress-strain relations of hyperelastic materials, according to equation (5), is the principal part of a user subroutine VUMAT. In this subroutine, the kind of model is planar shell. Next, the mode variables such as stress are defined in terms of strain in different directions. In the next section, constants for the program such as the Neo-Hookean coefficient parameter and the maximum stress failure and definition properties such as density and the number of parts to analyze are determined. Parts such as direct components (tensile and compressive stresses) or indirect components (shear stresses) perform a specific function. The user subroutine VUMAT is based on von Mises' original equation. The equation that was used is as follows:

$$\sigma_e = \left[\frac{3}{2}\left(\sigma_{11}^2 + \sigma_{22}^2 + \sigma_{33}^2 + 2\sigma_{12}^2 + 2\sigma_{23}^2 + 2\sigma_{31}^2\right)\right]^{1/2} \sigma_e\langle\sigma_{22} \tag{6}$$

This equation expresses the flow stress of material with parameters such as principal stresses and shear failure, tensile matrix mode, $\sigma_e < \sigma_{22}$, $\sigma_{11} = \sigma_{33} = 0$.The detailed flow chart of VUMAT for implementing progressive damage analysis is demonstrated in Fig. 6. The total calculation process of VUMAT is repeated in each material point of the elastomer matrix material of the composite laminates model. At every incremental step, the current strains were updated in line with the strain increment components which were transferred to VUMAT from ABAQUS. Then the current stresses were updated according to the

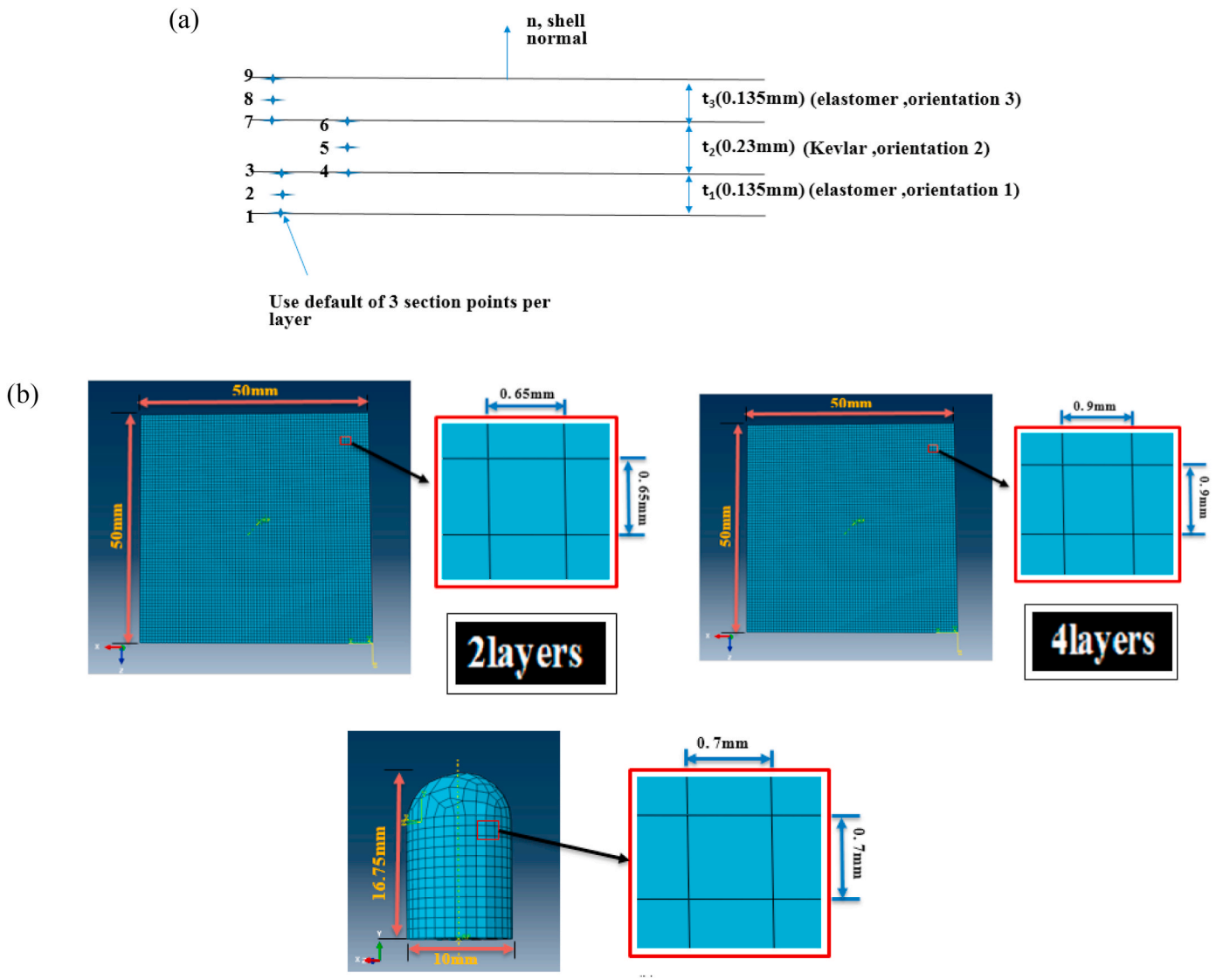


**Fig. 7.** (a) Shell element sample for 1-layer Kevlar/elastomer composite, (b) design details of the panel at different layers and projectile mesh.

corresponding constitutive model and current strains. Moreover, the degree of damage could also be evaluated in light of the current stresses. Once the failure criteria of von Mises' stress were reached, the stresses of each material point were updated according to the stress-strain relations of the hyperelastic material. Lastly, the updated state variables were returned to the main procedure ABAQUS for the next incremental step until the relevant element was eliminated or impact process ended.

### 3.1.2. *Fiber failure criterion*

Damage is the local separation of a material into pieces under the action of stress. Depending on conditions, the damage procedure can be brittle or ductile. In ductile damage, necking takes place before fracture. Transmission is slow with a comparatively large dissipation of released strain energy and crack face separation [63]. In addition to determining the behavior of Kevlar fabric from damage criteria such as ductile damage, ABAQUS software used the parameter fracture energy in the ductile damage to estimate the fracture of the fiber. Once the failure criteria of the fracture energy ($G_F$) were reached, the energy of each material point ($G_{Ff}$) was examined according to the fracture energy. Lastly, this process continued in ABAQUS for every incremental step until the relevant element was eliminated or the impact process ended. Fig. 6 gives a detailed flow chart for implementing progressive damage analysis in fiber.

### 3.2. *Modeling*

In this section, the simulations were accomplished by the most advanced method of modeling the finite element of composites, ABAQUS/Explicit with user-defined material models (VUMAT). For this purpose, each layer is modeled on a three-dimensional coordinate system and is deformable. Each section of the planar shell type with dimensions of 50 × 50 $mm^2$ and 0.5 mm thick was selected. Another part chosen in this simulation was the projectile, which was modeled with a discrete rigid part, introducing the projectile option of a completely rigid part. This option was used because the projectile resisted deformation. The model required a base point to which all the constraints and loads were assigned. In this study, this point was preferably determined at the bottom of the projectile. In ABAQUS, different layers of the composite laminate can be defined using the composite layout in the property section. Various thicknesses of the layers of the shell elements were determined. An example of a shell element definition with different layers is shown in Fig. 7a. In this figure, the type of material, the thickness, and the angle of each layer are distinguished.

In this study, a shell element in composite laminate was developed using the option "auto mesher: size mesh mode". Thus, the meshing shape was generated in a quadrilateral. Fig. 7b shows the panel mesh mode. To maintain the independent numerical solution of the meshing,

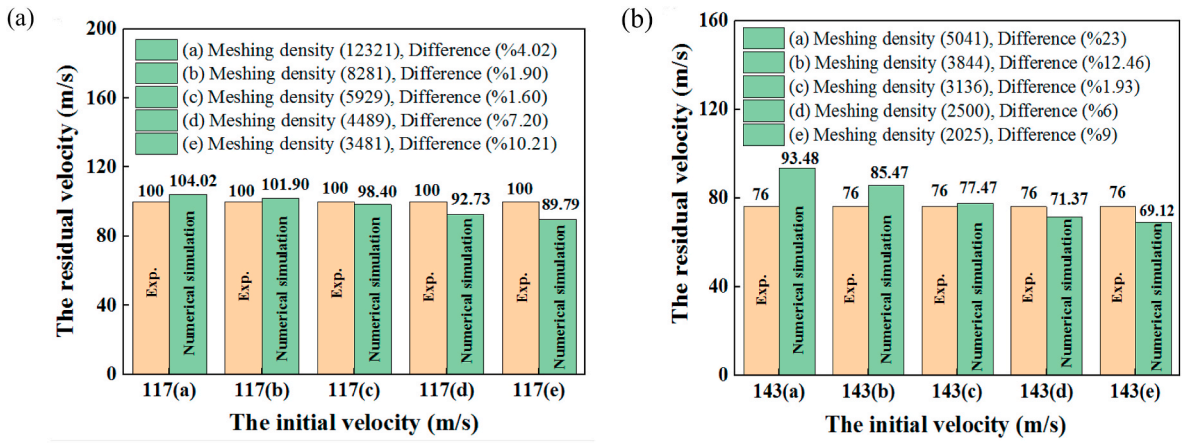


**Fig. 8.** Convergence of: (a) 2-layer composite with a thickness of 1 mm, (b) 4-layer composite with a thickness of 2 mm. Both sets of images show the best meshing density under the high-velocity impact.

**Table 6**
Physical and mechanical properties of the Kevlar fabric and elastomer [51,64].

| Material | Density (kg/m$^3$) | Neo -Hookean Constitutive model ($C_1$) (Mpa) | Poisson's ratio | Young's modulus (Mpa) | Ultimate tensile strength (Mpa) | Strain rate ($1/s^{-1}$) | Tensile fracture strain | Fracture energy (J) |
|---|---|---|---|---|---|---|---|---|
| Kevlar | 1440 | – | 0.25 | 83 | 2920 | 0.004 | 0.04 | 1343.2 |
| Elastomer | 950 | 0.99 | – | – | 9.56 | – | 0.023 | – |

the mesh convergence was studied to estimate the effect on the residual velocity of using different mesh modes. The convergent mesh values for different thicknesses were obtained in the model analysis.

The mesh sizes for different mesh modes, namely, 0.00045, 0.00055, 0.00065, 0.00075, and 0.00085 were investigated at a collision velocity of 117 m/s for a 2-layer composite with a thickness of 1 mm, and for mesh modes of 0.0007, 0.0008,0.0009, 0.0010, and 0.0011 were investigated at a collision velocity of 143 m/s for a 4-layer composite with a thickness of 2 mm. According to Fig. 8, in the five studied modes for these composites, the best case is for a 2-layer composite with a mesh size of 0.0065 and a meshing density of 5929, and for a 4-layer composite with a mesh size of 0.0009 and a meshing density of 3136.

The model presented in this study is an explicit dynamic model. It is also possible to analyze the components of this composite structure to assign the mechanical properties of the contact between them from the general contact in all the solution steps. A general collision with the

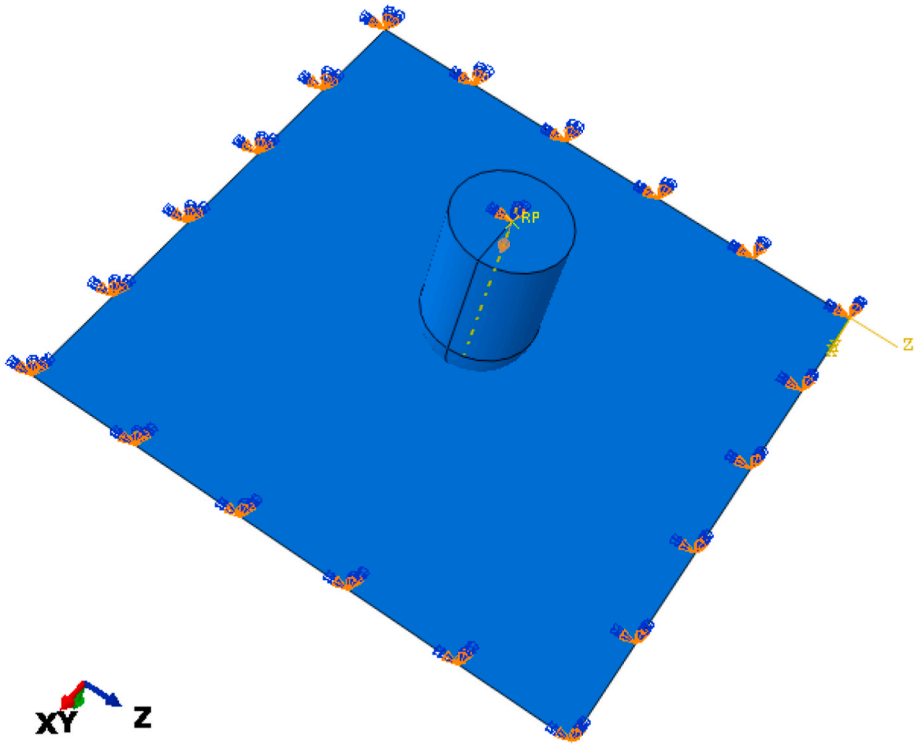


**Fig. 9.** Boundary conditions of flexible composite and projectile.

**Table 7**
Compare the velocity output of 2-layer composite with a thickness of 1 mm with different impact velocities during ballistic impact.

| Initial velocity (m/s) | Expt. residual velocity (m/s) | Numerical simulation residual velocity (m/s) | Difference (%) | Projectile diameter, $d_p$(mm) | Projectile mass, $m_p$ (gr) | Thickness of target (mm) |
|---|---|---|---|---|---|---|
| 117 | 100 | 98.40 | 1.60 | 10 | 9.32 | 1 |
| 122 | 104 | 102.53 | 1.41 | 10 | 9.32 | 1 |
| 125 | 106 | 106.69 | 0.65 | 10 | 9.32 | 1 |

**Table 8**
Compare the velocity output of 4-layer composite with a thickness of 2 mm with different impact velocities during ballistic impact.

| Initial velocity (m/s) | Expt. residual velocity (m/s) | Numerical simulation residual velocity (m/s) | | Difference (%) | Projectile diameter,$d_p$ (mm) | Projectile mass, $m_p$ (gr) | Thickness of target (mm) |
|---|---|---|---|---|---|---|---|
| 143 | 76 | 77.47 | 1.93 | 10 | 9.32 | 2 | |
| 147 | 82 | 83 | 1.21 | 10 | 9.32 | 2 | |
| 152 | 88 | 89.31 | 1.48 | 10 | 9.32 | 2 | |

coefficient of friction 0.2 was set [65]. There was also surface-to-surface interaction between the composite and the projectile. Also, to prevent sliding between the composite layers; hence, tie contact was considered. The restriction applied to the degrees of freedom of a projectile considered to be of the rigid body type. This constraint allowed us to restrict the movement of areas of a model to the motion of a reference point.

### 3.3. Material properties

Table 6 shows the properties of the Kevlar and elastomer, individually [51,64]. This table is also used for numerical modeling. The properties of the Kevlar material included density ($\rho$), Young's modulus ($E$), and maximum fracture energy. The properties intended for the elastomer material included density ($\rho$), the constant coefficient of the neo-Hookean model, and maximum stress failure. The failure model defined in ABAQUS software is such that we can predict the complete failure model for ductile-elastic materials (such as Kevlar fabric) with isotropic behavior. Table 6 gives Young's modulus for each fiber layer that is modeled as an isotropic material. The justification for this simple assumption is that the yarn is pulled by the longitudinal deformation of the fibers. Failure is determined by the hardening of the material and plays an essential role in the analysis of fiber-reinforced composite materials. The user sub-routine VUMAT was also been used to model the damage behavior of elastomeric material. Given the square of the composite dimensions, the properties were equal longitudinally and transversely. In this study, the properties in terms of thickness were assumed to be similar to the longitudinal and transverse states.

### 3.4. Boundary condition and loading

Matching the boundary conditions in the experimental tests, the four target sides were defined as wholly clamped, and the initial velocity of the projectile was described for the projectile reference point. The mass of the projectile was supposed to be centrally located at its reference point. Regarding the projectile, it should be noted that the projectile was allowed to move in all directions of the page during the execution of the program. Fig. 9 shows the boundary conditions of the panel.

## 4. Results and discussion

In this section, the effects of the projectile collision with the target center of the elastomeric composite are presented.

**Table 9**
Ballistic limit velocity results for Kevlar/elastomer composite.

| Expt. residual velocity (m/s) | Numerical simulation residual velocity (m/s) | Difference (%) | Projectile diameter,$d_p$ (mm) | Projectile mass, $m_p$ (gr) | The Thickness of target (mm) |
|---|---|---|---|---|---|
| 64 | 62.53 | 2.2 | 10 | 9.32 | 1 |
| 122 | 121.3 | 0.57 | 10 | 9.32 | 2 |

### 4.1. Study on the residual velocity

By comparing the velocities obtained from the experimental value presented in Tables 7 and 8, it can be seen that this model is a suitable solution for predicting the Kevlar/elastomer composite response to high-velocity impact. The rates of accuracy of the model in predicting the projectile residual velocity of the Kevlar/elastomer 2-layer composite at the velocities of 117, 122 and 125 m/s compared to the experimental results were respectively 1.60%, 1.41%, and 0.65% and its rates of accuracy in predicting the projectile residual velocity of the Kevlar/elastomer 4-layer composite at the velocities of 143, 147 and 152 m/s compared to experimental results were respectively 1.93%, 1.21%, and 1.48%. The results show that there was a decent level of agreement between the analytically predicted values and the experimental values.

### 4.2. Study of the ballistic limit

The velocity of the ballistic limit was predicted for different target thicknesses (see Table 9), using the numerical simulation presented in this study. This table shows the ballistic limits of 62.53 m/s and 121.30 m/s respectively for the composite two and four layers. In addition, the ballistic limit achieved from the numerical simulation was compared with the experimental results for the fabric Kevlar/elastomer composite. Good agreement can be seen between the numerical simulation results and the experimental observations.

This simulation entailed two steps. The first step was before the impact on the 4-layer elastomeric composite panel, and the second step related to the deformation after impact. These steps are shown in Fig. 10. The hemispherical projectile hit the four-layer panel at different initial velocities, and the residual velocities were calculated from the panel. In Fig. 10a, b and 10c, color views of the structure can be seen after the impact and deformation. The red color experienced the worst deformation, and blue color the least deformation at the impact site. Fig. 10d, also, shows the velocity of the projectile in the numerical simulation,

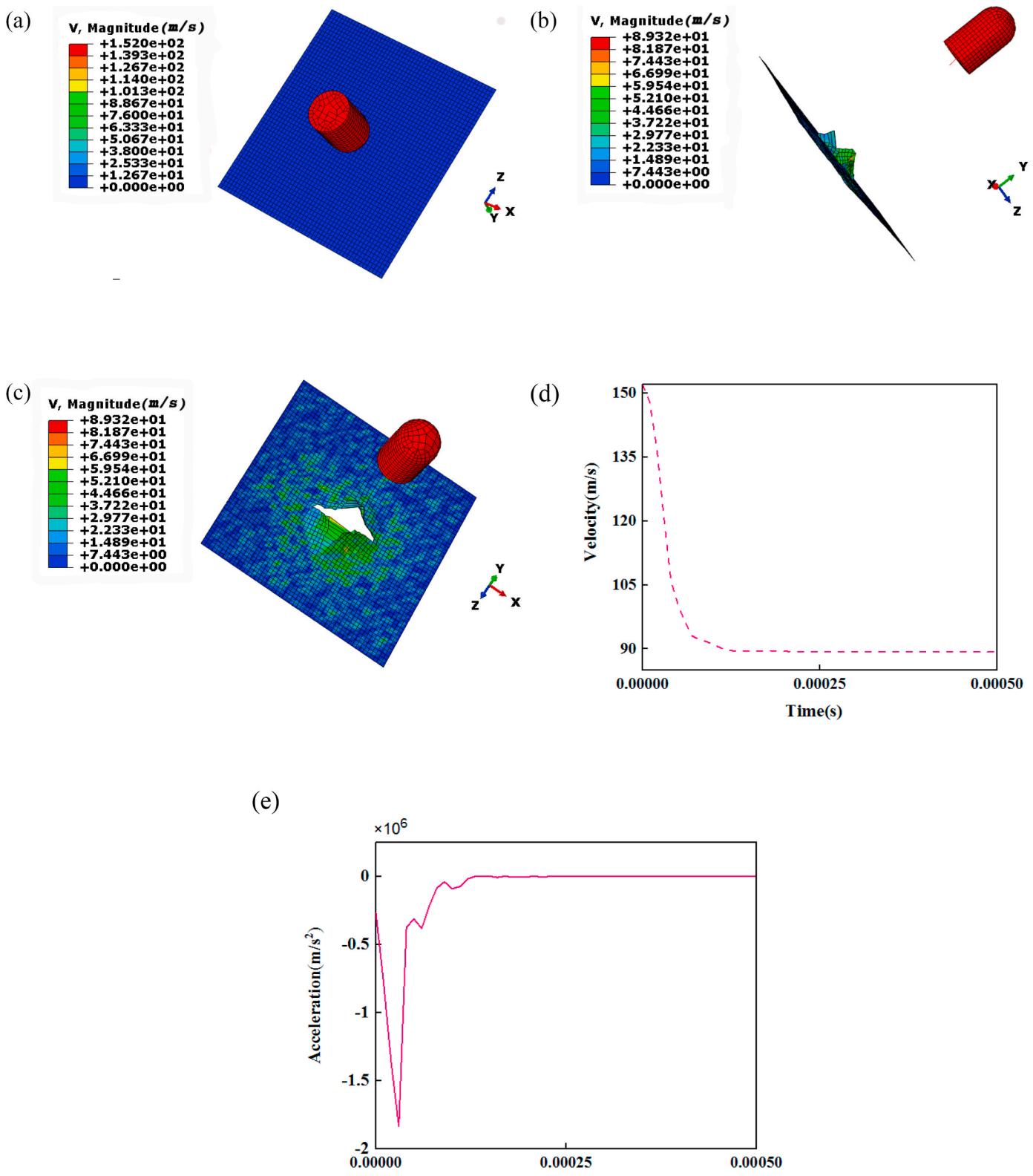


**Fig. 10.** The penetration of a projectile with an initial velocity of 152 m/s on the 4-layer Kevlar/elastomer composite of 50 × 50 $mm^2$ dimensions: (a) before impact, (b) after impact from a side view, (c) after impact from the front, (d) the velocity output, (e) the acceleration output.

initially 152 m/s along the vertical axis. According to Fig. 10d and e, the deformation velocity and acceleration of the projectile in the vertical axis direction take 0.002 s after the collision. As can be seen in Fig. 10d, the structure changes rapidly in the first few milliseconds. But after 0.15 ms, the rate of deformation of the composite structure decreases in a slow slope, to the point where it becomes uniform. In fact, the reason for the slowdown is the deformation of the impact areas. First, the composite structure absorbs the impact force by becoming deformed until the affected areas are damaged, and the plates are torn. When the plates are stretched to their limit, deformation is reduced, and the force applied

**Table 10**
Comparison between the velocity output of 2-layer Kevlar/elastomer composite with different dimensions using. numerical simulation.

| The target dimension ($mm^2$) | The initial velocity (m/s) | Numerical simulation residual velocity (m/s) | Projectile diameter,$d_p$ (mm) | Projectile mass, $m_p$ (gr) | Thickness of target (mm) |
|---|---|---|---|---|---|
| 50 × 50 | 117 | 98.40 | 10 | 9.32 | 1 |
| | 122 | 102.53 | 10 | 9.32 | 1 |
| | 125 | 106.69 | 10 | 9.32 | 1 |
| | 117 | 86.46 | 10 | 9.32 | 1 |
| 100 × 100 | 122 | 96.43 | 10 | 9.32 | 1 |
| | 125 | 98.75 | 10 | 9.32 | 1 |

**Table 11**
Comparison between the velocity output of 4-layer Kevlar/elastomer composite with different dimensions using numerical simulation.

| The target dimension (m/s) | The initial velocity (m/s) | Numerical simulation residual velocity (m/s) | Projectile diameter,$d_p$ (mm) | Projectile mass, $m_p$ (gr) | Thickness of target (mm) |
|---|---|---|---|---|---|
| 50 × 50 | 143 | 77.47 | 10 | 9.32 | 2 |
| | 147 | 83 | 10 | 9.32 | 2 |
| | 152 | 89.31 | 10 | 9.32 | 2 |
| | 143 | 66.81 | 10 | 9.32 | 2 |
| 100 × 100 | 147 | 74.42 | 10 | 9.32 | 2 |
| | 152 | 87.68 | 10 | 9.32 | 2 |

**Table 12**
Compare the amount of energy absorbed during ballistic impact of different velocities on the Kevlar./elastomer 50 × 50 mm2 composite.

| Number of layers | Initial velocity (m/s) | Expt.energy absorbed(J) | Numerical simulation energy absorbed (J) | Difference (%) |
|---|---|---|---|---|
| 2- layer | 117 | 17.19 | 18.67 | 8.6 |
| | 122 | 18.95 | 20.37 | 7.4 |
| | 125 | 20.52 | 19.76 | 3.7 |
| | 143 | 68.37 | 67.32 | 1.53 |
| 4- layer | 147 | 69.36 | 68.59 | 1.11 |
| | 152 | 72.99 | 70.49 | 3.42 |

to the structure is used only to break it. Also, in dynamic loading after a projectile impact, at a time step of 0.002 s, acceleration is extracted as a function of time. According to Fig. 10e, in the case of high-velocity impact, the increase of the peak area related to the acceleration of this composite shows more energy absorption. When the peak length of the acceleration diagram increases, the projectile experiences more time in contact with the composite target At this time, the velocity of the projectile is sharply reduced. In the numerical simulation, the same mesh density was used to check the residual velocity of the hemispherical projectile with a mass of 9.32 g, a length of 16.75 mm, and a diameter of 10 mm in collision with a 2-layer composite Kevlar/elastomer target with dimensions of 100 × 100 $mm^2$. Tables 10 and 11 show the comparison of the results of the residual velocity on the 2- and 4-layer Kevlar/elastomer composite targets with different dimensions.From the above tables, it can be concluded that in this numerical simulation, by increasing the target dimensions and maintaining the same initial velocities, the residual velocity of the impact increases and energy absorption declines. It can be seen in Tables 6 and 7 that the residual velocity and energy of the projectile are reduced.

### 4.3. Investigation of energy absorption

The kinetic energy absorbed from the projectile to the target plate is

**Table 13**
Compare the amount of energy absorbed at different velocities on the 2- layer Kevlar/elastomer composite for. different dimensions.

| Target dimension ($mm^2$) | Initial velocity (m/s) | Numerical simulation energy absorbed (J) | Projectile diameter,$d_p$ (mm) | Projectile mass, $m_p$ (gr) | Thickness of target (mm) |
|---|---|---|---|---|---|
| 50 × 50 | 117 | 18.67 | 10 | 9.32 | 1 |
| | 122 | 20.37 | 10 | 9.32 | 1 |
| | 125 | 19.76 | 10 | 9.32 | 1 |
| | 117 | 28.95 | 10 | 9.32 | 1 |
| 100 × 100 | 122 | 26.02 | 10 | 9.32 | 1 |
| | 125 | 27.37 | 10 | 9.32 | 1 |

**Table 14**
Compare the amount of energy absorbed at different velocities by the 4-layer Kevlar/elastomer composite for different dimensions.

| Target dimension ($mm^2$) | Initial velocity (m/s) | Numerical simulation energy absorbed (J) | Projectile diameter,$d_p$ (mm) | Projectile mass, $m_p$ (gr) | Thickness of target (mm) |
|---|---|---|---|---|---|
| 50 × 50 | 143 | 67.32 | 10 | 9.32 | 2 |
| | 147 | 68.59 | 10 | 9.32 | 2 |
| | 152 | 70.49 | 10 | 9.32 | 2 |
| | 143 | 74.49 | 10 | 9.32 | 2 |
| 100 × 100 | 147 | 74.88 | 10 | 9.32 | 2 |
| | 152 | 71.38 | 10 | 9.32 | 2 |

equal to:

$$E = \frac{1}{2} m_p \left(V_0^2 - V_r^2\right) \tag{7}$$

where $m_p$ is the mass of the projectile, $V_r$is the residual velocity of the projectile, $V_0$ is the velocity of the ballistic limit. Table 12 shows separately the energy absorbed in the 2- and 4-layer laminates during impact. By comparing the energy absorption obtained from the experimental value and in the numerical model presented in these tables, it can be seen that this model is a suitable solution for the Kevlar/elastomer composite with different thicknesses. The accuracy of the model in predicting the absorbed energy of the Kevlar/elastomer 2- layer composite at the velocities of 117, 122, and 125 m/s compared to the experimental results is respectively 8.6%, 7.4%, and 3.7% and in predicting the energy absorbed of the Kevlar/elastomer 4-layer composite at the velocities of 143, 147, and 152 m/s compared to the experimental results is respectively 1.53%, 1.11%, and 3.42%. This accuracy produces a good match between the experimental values and those of the numerical model.

Tables 13 and 14 also summarize the energy absorption of the 2- and 4-layer Kevlar/elastomer composites with dimensions of 50 × 50 $mm^2$ and 100 × 100 $mm^2$ at the initial velocities of impact. It can be observed that, by increasing the target dimensions due to the presence of more elements, and the contact force between the projectile and the target, the amount of energy absorbed increases and the failure of the composite reduces. During ballistic impact, the impact velocity decreases because it comes into contact with the composite structure. This reduction in the projectile is associated with the reaction force on the projectile because the kinetic energy is transferred to the composite structure. Therefore, increasing the flexibility of the composite structure increases the energy that is absorbed.

### 4.4. Deformation and mechanisms of damage

Fig. 11 presents the response of the experimental and numerical model of the fabric Kevlar/elastomer composite to the impact of high

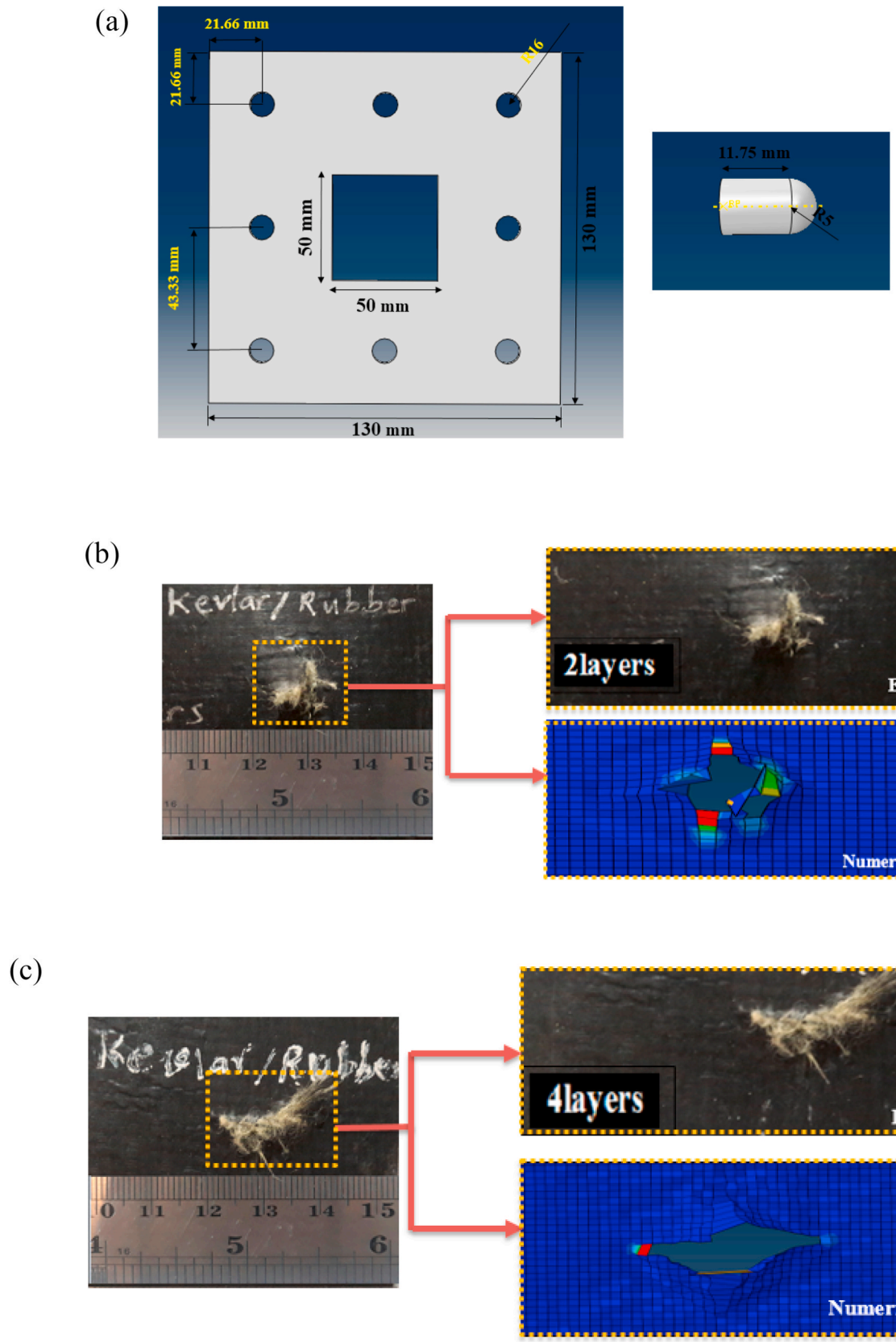


**Fig. 11.** (a) Schematic of fixture used for ballistic tests and technical drawing of projectile, (b) Front view of Kevlar/elastomer 2-layer composite after perforation at the impact velocity of 125 m/s with the experimental and the numerical model, (c) Front view of Kevlar/elastomer 4-layer composite after perforation at the impact velocity of 152 m/s with the experimental and the numerical model.

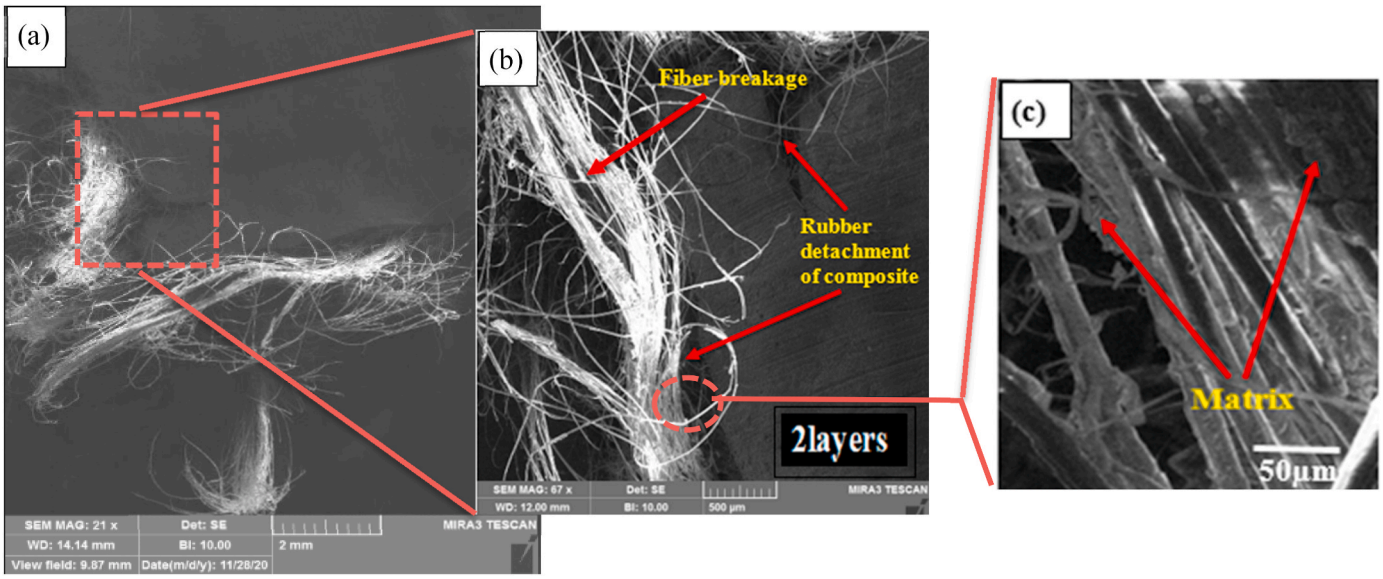


**Fig. 12.** SEM images of the Kevlar/elastomer 2- layer composite: (a) SEM images with 2 mm scale shows the failure of composite after perforation at the impact velocity of 125 m/s, (b) SEM zoom with 500 µm scale showing closely the fiber breakage and rubber detachment of composite, (c) the high-resolution SEM observation with 50 µm scale showing the matrix attached to fiber after the test.

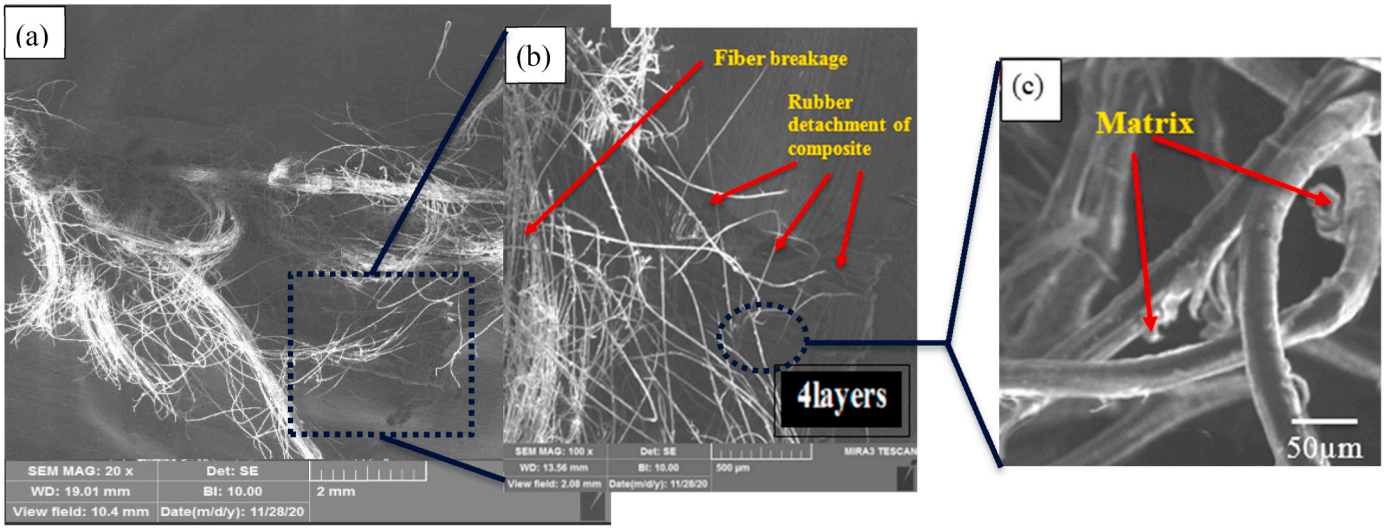


**Fig. 13.** SEM images of the Kevlar/elastomer 4- layer composite: (a) SEM images with 2 mm scale shows the failure of composite after perforation at the impact velocity of 125 m/s, (b) SEM zoom with 500 µm scale showing closely the fiber breakage and rubber detachment of composite, (c) a closer SEM zoom with 50 µm scale showing the matrix attached to fiber after the test.

velocity and shows the front face of each sample. The layers are associated and effectively resist a hemispherically nosed projectile, due to the presence of rubber. A small amount of delamination can be observed between the plies. It can be seen that the impact event is successfully captured in the experimental and numerical simulation.

Some of the most critical aspects of a polymer composite are the strength and stability of the fiber/matrix bond [66]. As the flexibility of elastomeric composite structure increases, the strength of the bond begins to be excessive, so the material fails to some extent in a manner to do with traction. But if the bond is too weak, properties such as fiber breakage resistance and compression strength are compromised. In the structure of composites, the fibers are activated in a boost that bonds them to the surrounding matrix. Unfortunately, because the sensitive fiber/matrix bond is sensitive to environmental factors, such as temperature, moisture, and manufacturing aberrations such as alterations in the fiber surface treatment, the composites are damaged. Figs. 12 and 13 show the damage mechanism of the Kevlar/rubber composites of 2 and 4 layers under impact loading based on the SEM micrographs. The electron microscope images of specimens acquired at lower magnifications allow us to compare the applied methods in the quality of the interfacial bonding between the fibers and matrix. The SEM of both types of composite sample during ballistic impact are illustrated in Figs. 12 and 13, where noticeably indicated fiber breakage can be seen. The detachment of the rubber matrix which was induced under impact loading by the further fiber breakage was also observed along one dimension and perpendicular to it.

From the experimental results discussed in the previous section, the damage process for all specimens exhibits roughly similar characteristics, so specimens 2-and 4-layer were chosen to show the deformation and damage profile in the high-velocity impact (see Fig. 14). From the experimental and numerical results, it is obvious that only the contact area between the specimen and projectile was damaged, but the non-

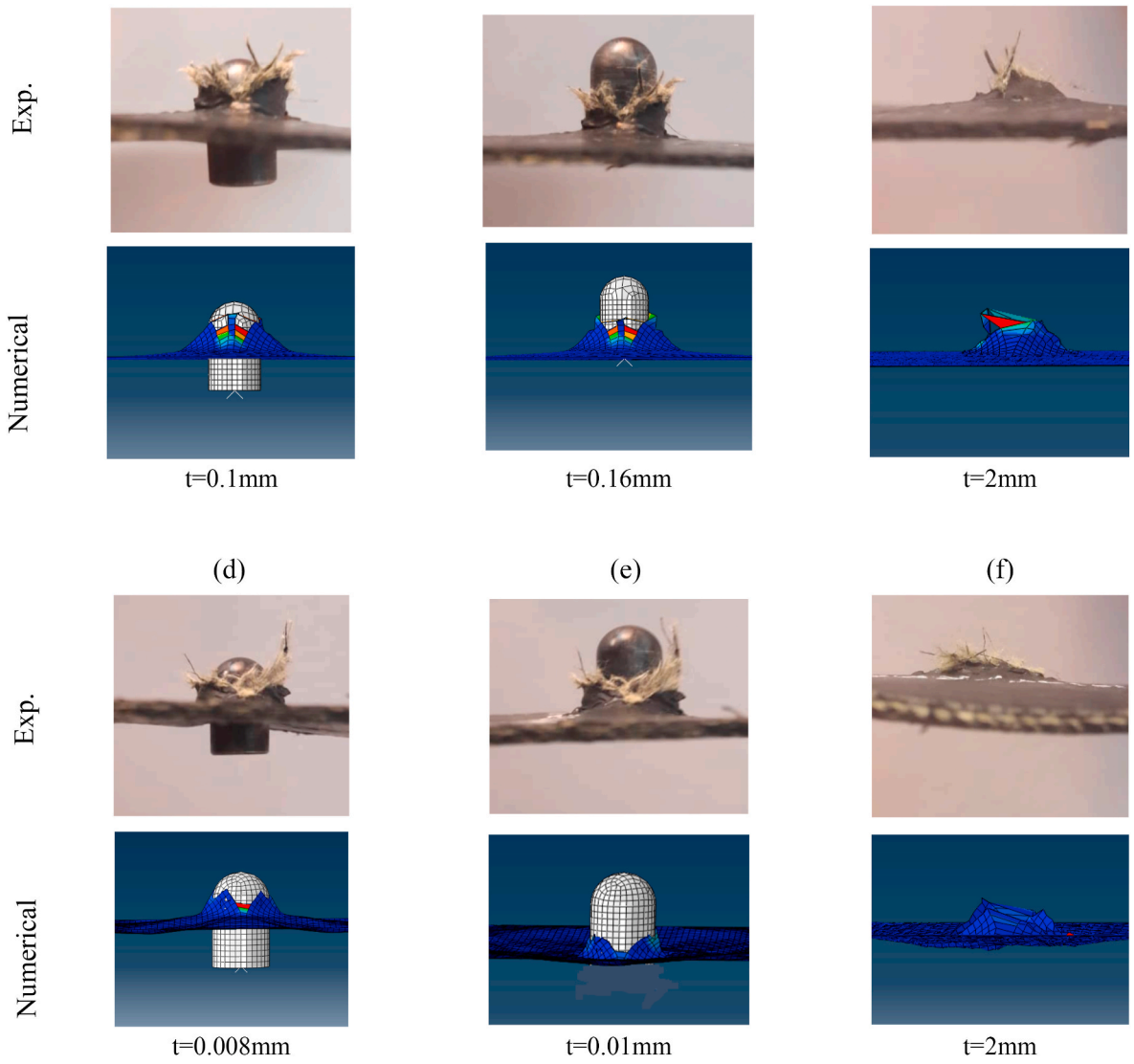


**Fig. 14.** Comparison of penetration of the projectile in the experimental and the numerical model of the: (a–c) Kevlar/elastomer 2- layer composite, (d–f) Kevlar/elastomer 4- layer composite. Both sets of images show the progressive deformation and damage under the high-velocity impact at different times.

impact area shared the energy absorption as the impact velocity increased. The deformation of the panel experienced both global and local displacements during impact process. The global displacement was mainly caused by extensive flexibility in the panel due to the elastomer matrix, whereas the local displacement was primarily triggered by the projectile in the impact area. The local and global deformations indeed interacted; as the panel collapsed in the local deformation, the global deformation helped to delay the final failure in the longitudinal fibers accompanied inter- and intra-lamina and the detachment of the rubber matrix.

### 4.5. Investigation of damage mechanics

Fig. 15 shows the greatest damage due to tensile stresses at the projectile impact point; the resulting material orientation is defined for the composite plate model. Fig. 15 shows *X*-in the fiber direction; *Y*- in the thickness direction (in the direction of the applied load); and *Z*-in the transverse direction. According to the experimental results in the previous section and the numerical model tensile failure of the fibers occurred as the primary mechanism of destruction in this structure, due to the lack of failure mechanisms such as layered separation, matrix separation from fibers, and cracking in this composite. It can be seen that the presence of elastomer, unlike the thermoset matrix [61], had enough flexibility to prevent the spread of damage in the composite and absorb more energy. Fig. 15 also shows the positive effect of the elastomer matrix on the Kevlar fabric in the composite, which allows the fiber in both the impact area and the non-impact area to participate in the energy absorption of the projectile. This delayed the failure in the impact zone because of the greater energy of the flexible elastomer matrix. Further, increasing the thickness of the composite made the fiber yarns thicker and more effective in improving the damage resistance and reducing the residual velocity of the projectile.

To evaluate the effect of impact energy on fiber damage, the failure energy criterion of formable materials was used. The results of the failure energy criterion of fiber in 4-layer elastomeric composites are shown in Fig. 16. The status of damage corresponded to the effect of the particular damage variable ranging from 0 to 1, where 0 indicates that the element was not yet damaged. In contrast, the amount of 1 indicates that damage occurred to the element according to the failure energy criterion.

Fig. 17 shows that as the initial velocity of projectile increases, greater force is applied to the composite, and consequently more von Mises' stress is created in the composite.

The simple assumption is that when the yarn is pulled by the

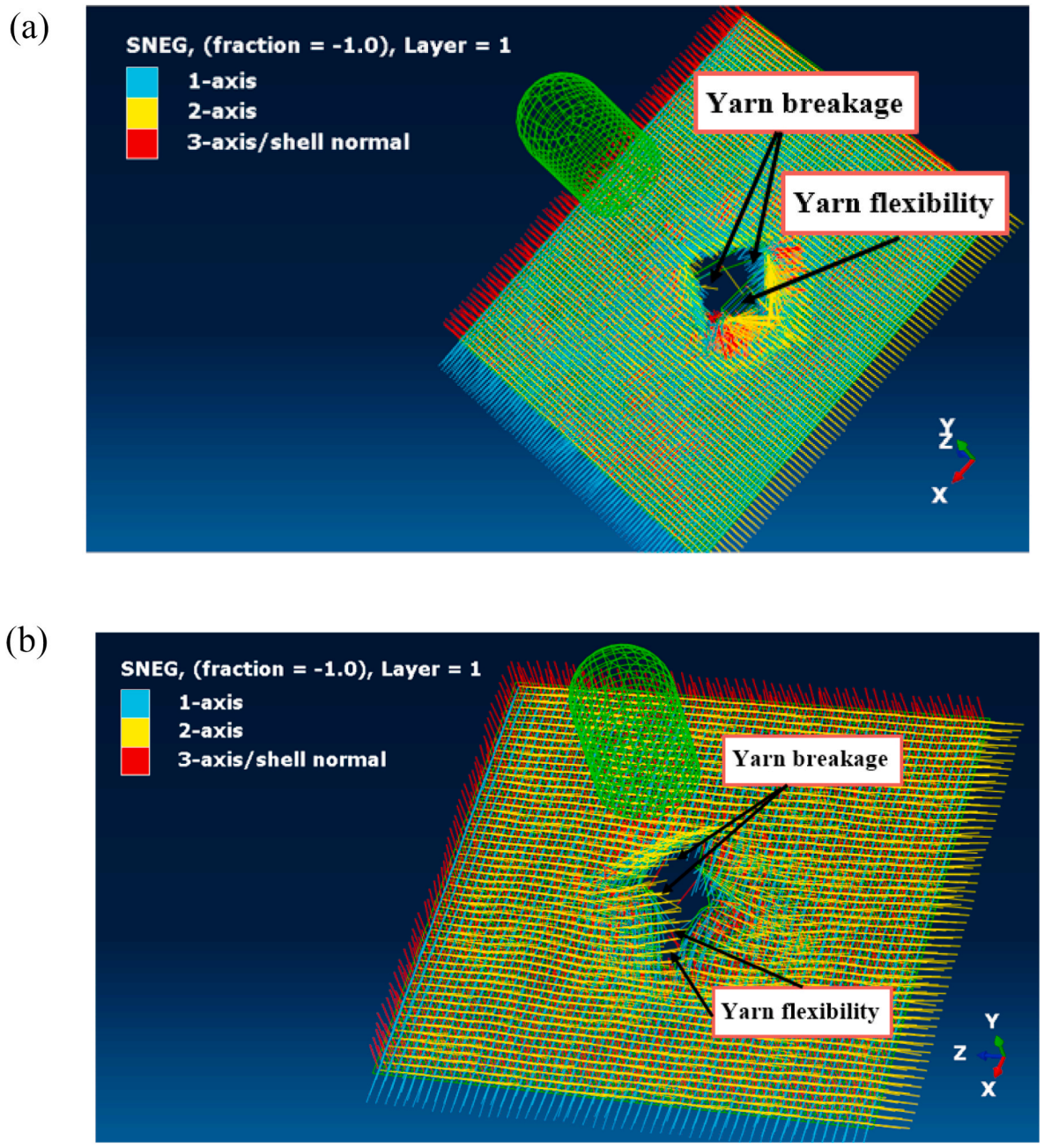


**Fig. 15.** Resulting material orientation defined for the numerical model of the: (a) 2-layer composite, (b) 4-layer composite. Both sets of images displaying the damage of yarn under high-velocity impact and their resistance with increasing layers.

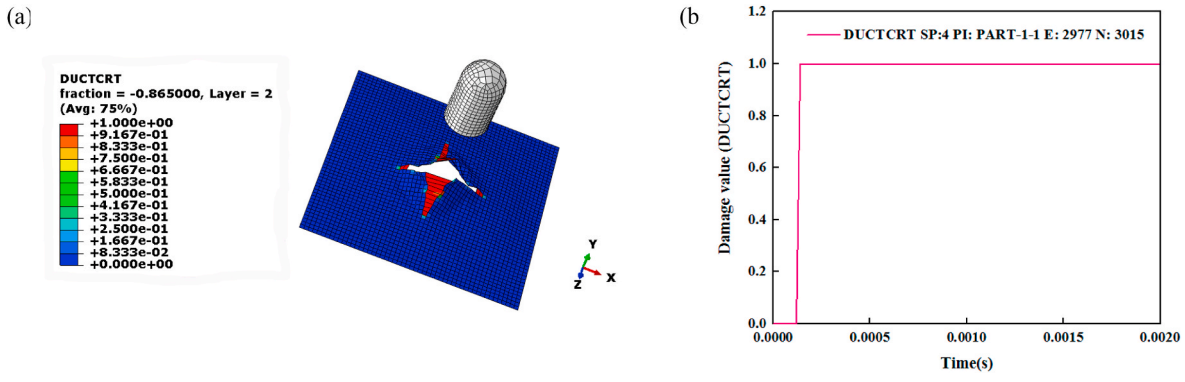


**Fig. 16.** (a) The failure energy of fiber of the elastomeric composite at the numerical model, (b) damage values a time step of 0.002 s for a particular element.

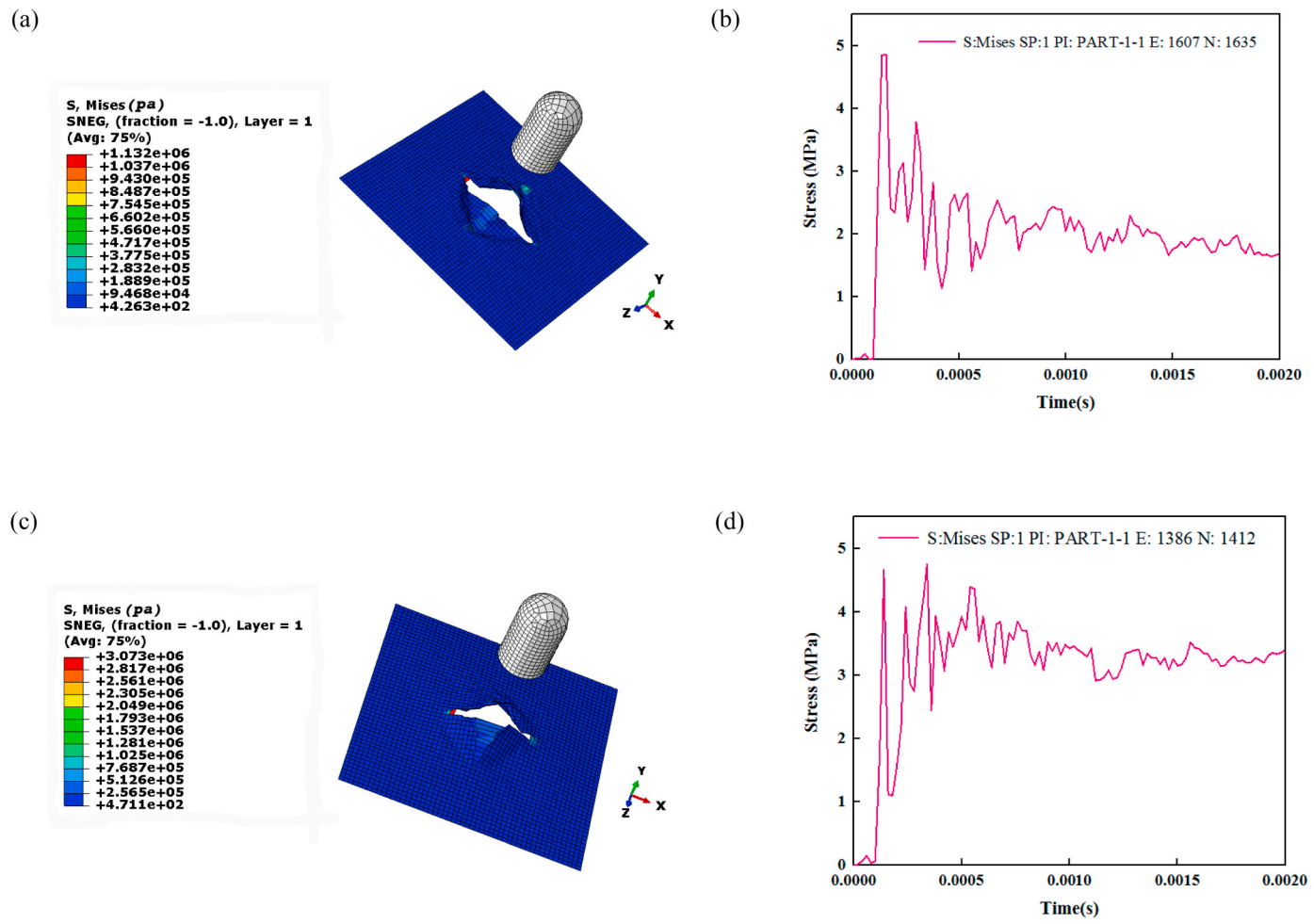


**Fig. 17.** Numerical estimations of the amount of von Mises' stress on the Kevlar/elastomer 4-layer composite with the stress output for a particular element under high-velocity impact with: (a–b) an initial velocity of 143 m/s with, (c–d) an initial velocity of 152 m/s.

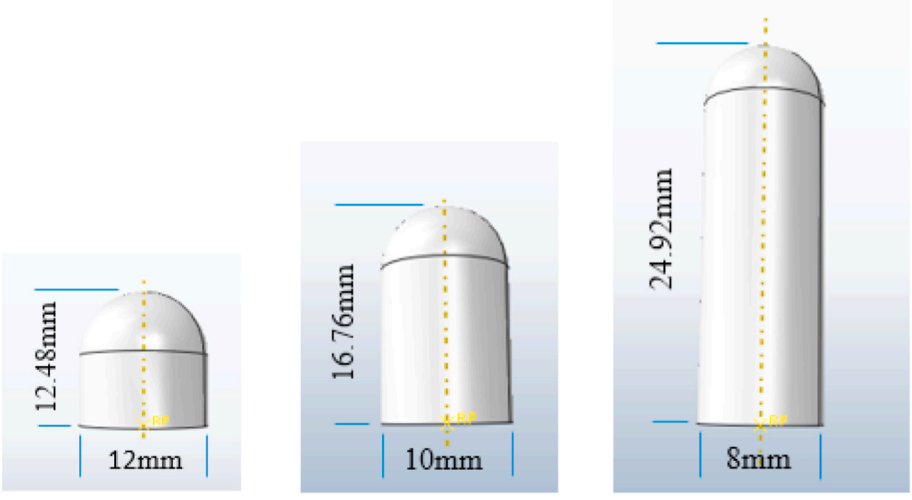


**Fig. 18.** Graphic representation of the shapes and dimensions of various projectiles used in numerical simulations.

longitudinal deformation of the fibers, the von Mises' stresses due to the impact of the projectile on the thickness of the composite can be investigated. During the ballistic impact, the impact velocity decreases due to the contact of the projectile with the composite structure, the reaction force on the projectile, and the kinetic energy transferred to the composite structure. According to Fig. 17, in 0.0002 s after the impact, many elements were removed from the composite because the stress of these elements exceeded the permissible strength. So, it must be noted that, the stress on these elements is affected by the compressive stresses under the projectile site and the tensile stresses around them, which it

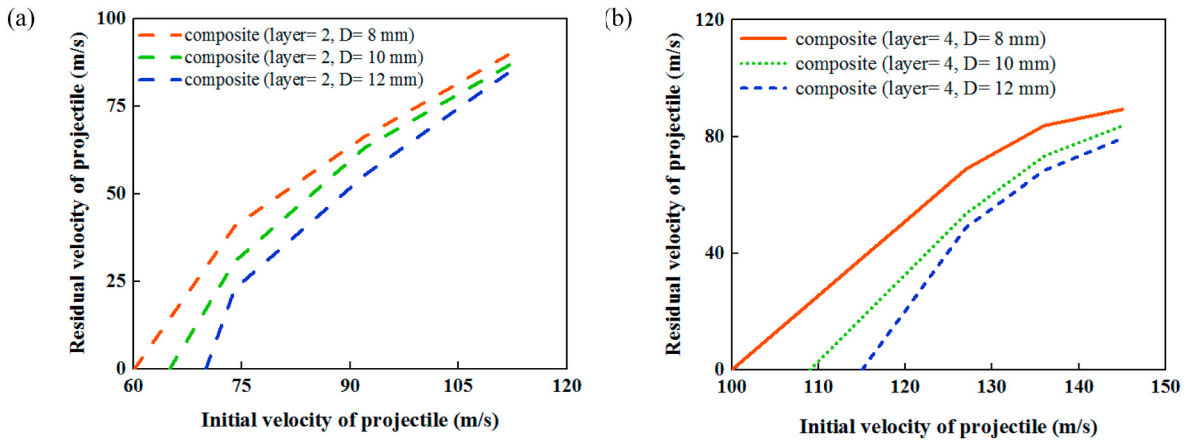


**Fig. 19.** Residual velocities at different impact velocities with projectiles of various dimensions: (a) on the 2- layer Kevlar/elastomer composite, (b) on the 4-layer Kevlar/elastomer composite. Both sets of images showing the effect of the projectile diameter on the residual velocity.

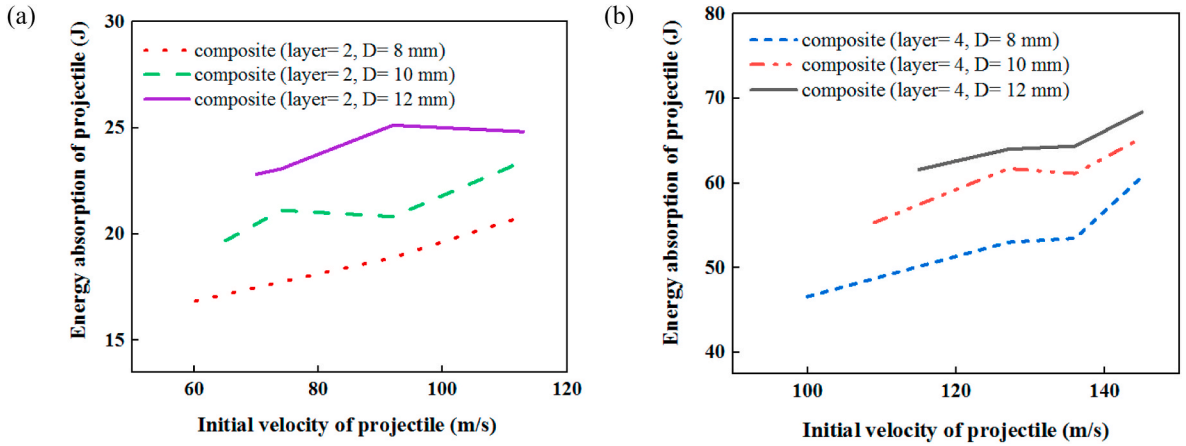


**Fig. 20.** The effect of the projectile diameter on energy absorption at the different impact velocities: (a) on the 2-layer Kevlar/elastomer composite with 1 mm thickness, (b) on the 4-layer Kevlar/elastomer composite with 2 mm thickness.

causes to increase to their limits. Furthermore, as the number of composite layers increases, the stress on the elements will increase. This causes the elements to fail under greater stress and the composite failure to be postponed.

## 5. Investigating the impact of projectile shape on the penetration rate

The shape of a projectile is the main factor in the amount of energy absorbed and impact resistance by the elastomeric composite. Thus, the impact resistance of these composites against hemispherical projectiles of different length to diameter ratios is compared in the numerical model. In this study, the effect of projectile diameter is analyzed using three different geometries, as shown in Fig. 18. In all shapes, the mass of the projectiles is m = 9.32 g.

Fig. 19 shows a comparison of projectiles with diameters of 8, 10, and 12 mm to evaluate in turn the residual velocity of the projectile from 2- and 4-layer composite Kevlar/elastomer targets. It is shown that increasing the diameter of the projectile reduces the residual velocity. It can also be seen in Fig. 19 that the lowest residual velocity is related to the projectile when the diameter is 12 mm, while the highest residual velocity is obtained from the projectile when the diameter is 8 mm. Therefore, the composite panel is more resistant to projectiles with a diameter of 12 mm. At the same initial velocity, the residual velocity of a projectile with a diameter of 12 mm is also lower than that of the other projectiles (with diameters of 8 and 10 mm), while projectiles with a larger diameter have a higher ballistic velocity. As a result of their shape, increasing the initial velocity reduces the difference between the residual velocity and the initial velocity of projectiles with different diameters.

Fig. 20 shows the energy absorbed by different diameters for 2- and 4-layer composite Kevlar/elastomer targets. According to these figures, the energy absorption of the elastomeric composite increases with increasing projectile diameter. In other words, increasing the contact surface of the projectile on the target causes the energy absorption to increase.

Fig. 21 displays the predicted fiber breakage under tensile stress during each impact event for different projectiles and the effect of the projectile shape on this composite. As illustrated in Fig. 21, the elements in the center area (impact area) of this composite – the fault zone – will be removed from the simulation. According to Fig. 21, the elements below the impact area of the projectile are mainly affected by tensile and shear stresses. The predominant failure mode in the impact of a hemispherical projectile on the target is tensile failure. Therefore, the projectile during penetration created great strains in the target responsible for the fiber breakage and the failure at the impact area. This failure was dominated by the process of high-velocity piercing, as in the case of a hemispherical projectile. The hemispherical end was able to perforate the target more easily by the process of piercing. The projectile damaged the target plate by fiber breakage under tensile stress. This is because the fiber breakage from tensile stresses is facilitated by increasing the diameter of the projectile; the stresses are generated between adjacent

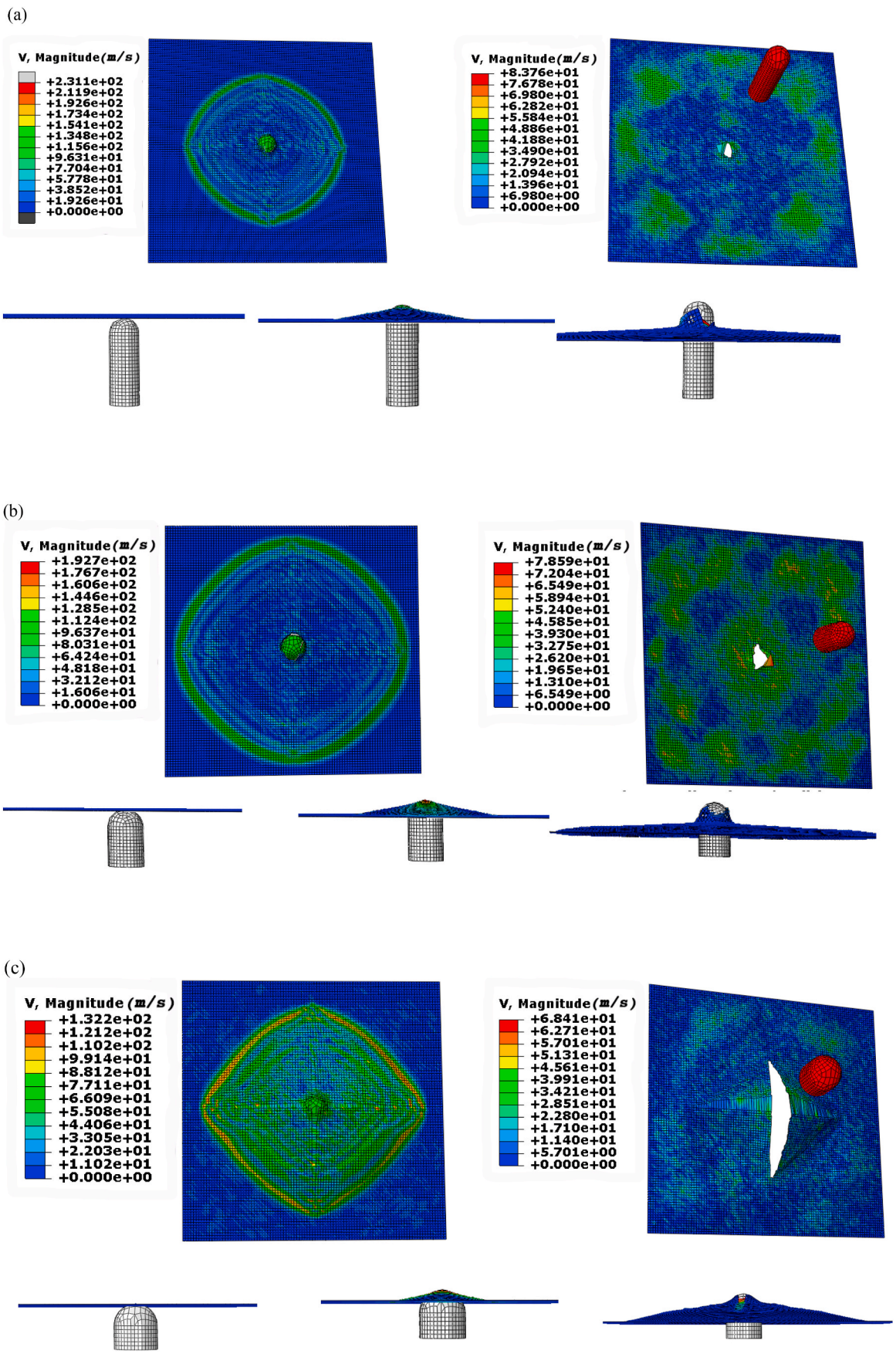


**Fig. 21.** Predicted deformation characteristics of Kevlar/elastomer composite: (a) projectile with a diameter of 8 mm, (b) projectile with a diameter of 10 mm, and (c) projectile a with diameter of 12 mm.

layers. Then the increase of fiber breakage causes the damaged area to expand and energy absorption to increase, due to the greater contact surface of the projectile inside the target. This energy absorbed appears to damage the composite target.

## 6. Conclusions

In this study, the high-velocity impact behavior of composite Kevlar/elastomer was investigated. For this purpose, the composite samples were 2- and 4-layer. According to the results, the composite Kevlar/elastomer has a high energy absorption rate due to the high strength of the fabric, the high flexibility of the elastomer, and their high impact resistance. The elastomer plays a crucial role in transmitting the kinetic energy of the projectile and its shock wave to the target. Hence, the presence of elastomer not only prevented the fabric from deforming, but also caused the fabric to experience its maximum tension and absorb more energy. From the experimental and numerical results of the present work, some important conclusions can be summarized as the following features:

- The test simulations indicated that by increasing the thickness of the composite, the fiber yarns became thicker and thus more effective in resisting damage and reducing the residual velocity of the projectile. Moreover, the experimental results showed that increasing the thickness of the composite increased the ballistic limit velocity and that increasing the $L/D$ ratio in the dynamic loading reduced the strain rate and stress levels. Furthermore, increasing the strain rate increased the stress levels, which demonstrates their dependence on the strain rate.
- During ballistic impact, in high strain rates, these composites exhibited non-linear behavior and high flexibility, which causes the rate of failure strain after the impact to go down and, consequently, more energy to be absorbed. Based on the results of the SEM investigations, the most usual damage mechanisms for 2- and 4-layer composite are fiber breakage and the detachment of the rubber matrix under impact loading. During ballistic impact, if the tensile strength of yarns exceeds the permissible tensile strength, eventually, the fibers break. The detachment of the rubber matrix was also observed after fiber breakage.
- Furthermore, as the number of composite layers increases, the stress on the elements will increase. This causes the elements to fail under greater stress, and the composite failure to be postponed. By increasing the target dimensions due to the presence of more elements, and the contact force between the projectile and the target, the amount of energy absorbed increases and the failure of the composite reduces.
- This work highlighted the elastomer matrix's positive effect on the Kevlar fabric in the composite, allowing to delay the impact zone's failure because of the more incredible energy of the flexible elastomer matrix. According to the numerical model results, the elastomer's presence, unlike the thermoset matrix [61], had enough flexibility and behaviour non-linear to avoid the spread of damage in the composite and absorb more energy. This matrix also caused the tensile failure of fibers of the primary destruction mechanism and did not experience failure mechanisms such as layered separation, matrix separation from fibers, and cracking in this composite. Further, increasing the composite thickness caused the fiber yarns to be thicker and more effective for developing the damage resistance and the energy absorption ability.
- The study showed that the deformation of the projectile had an excessive effect on the energy absorption of the target. Specifically, when the projectile diameter increased, the energy absorption of the target such as the energy absorption of the tensile failure of the fiber and the energy absorption of the separation of the elastomer from the composite increased due to the greater contact surface of the projectile.
- The present numerical modeling of elastomeric composites can accurately estimate the various damage mechanisms and energy absorption of this non-linear structure. In the proposed finite element model, an attempt was made to provide a simple, efficient, and accurate model by designing damage mechanisms and failure models to be used in other non-linear structures in the engineering sciences. Finally, there was a difference between the numerical and the experimental results. The error of this model in this comparison is, however, below 4%, which is acceptable in engineering calculations, and it was shown that the validated numerical model was able to simulate perforation and parametric studies.

## Author statement

S.Samane Asemeni: Conceptualization, Methodology, Investigation, Writing - original draft. Gholamhossein Liaghat: Conceptualization, Supervision, Methodology, Project administration, Writing - review & editing. Hamed Ahmadi: Supervision, Writing - review & editing. Yavar Anani: Supervision, Writing - review & editing. Amin Khodadadi: Review & editing. Sahand Chitsaz Charandabi: Review & editing.

## Declaration of competing interest

The authors declare that they have no known competing financial interests or personal relationships that could have appeared to influence the work reported in this paper.

## Acknowledgement

The authors gratefully acknowledge the help of Bu-Ali Sina University and Tarbiat Modares University in providing the necessary experimental facilities and technical support.

## References

[1] A.P. Sharma, S.H. Khan, R. Velmurugan, Effect of through thickness separation of fiber orientation on low velocity impact response of thin composite laminates, Heliyon 5 (2019), e02706.
[2] E.C. Botelho, R.A. Silva, L.C. Pardini, M.C. Rezende, A review on the development and properties of continuous fiber/epoxy/aluminum hybrid composites for aircraft structures, Mater. Res. 9 (3) (2006) 247–256.
[3] E. Carrera, Theories and finite elements for multilayered, anisotropic, composite plates and shells, Arch. Comput. Methods Eng. 9 (2) (2002) 87–140.
[4] M. O'Masta, B. Russell, V. Deshpande, An exploration of the ballistic resistance of multilayer graphene polymer composites, Extreme Mech. Lett. 11 (2017) 49–58.
[5] I. Lapczyk, J.A. Hurtado, Progressive damage modeling in fiber-reinforced materials, Composites Part A Appl. Sci. Manuf. 38 (11) (2007) 2333–2341.
[6] S. Li, X. Guo, J. Liao, Q. Li, G. Sun, Crushing analysis and design optimization for foam-filled aluminum/CFRP hybrid tube against transverse impact, Compos. B Eng. 196 (2020), 108029.
[7] L. Yao, G. Sun, W. He, X. Meng, D. Xie, Investigation on impact behavior of FMLs under multiple impacts with the same total energy: experimental characterization and numerical simulation, Compos. Struct. 226 (2019), 111218.
[8] G. Zhu, G. Sun, H. Yu, S. Li, Q. Li, Energy absorption of metal, composite and metal/composite hybrid structures under oblique crushing loading, Int. J. Mech. Sci. 135 (2018) 458–483.
[9] J.M. Alexander, An approximate analysis of the collapse of thin cylindrical shells under axial loading, The Quarterly Appl. Math. Mech. 13 (1) (1960) 10–15.
[10] W. Abramowicz, T. Wierzbicki, Axial Crushing of Multicorner Sheet Metal Columns, 1989.
[11] A. Singace, H. Elsobky, Further experimental investigation on the eccentricity factor in the progressive crushing of tubes, Int. J. Solid Struct. 33 (24) (1996) 3517–3538.
[12] M. Langseth, O. Hopperstad, Static and dynamic axial crushing of square thin-walled aluminium extrusions, Int. J. Impact Eng. 18 (7–8) (1996) 949–968.
[13] G. Sun, H. Zhang, J. Fang, G. Li, Q. Li, A new multi-objective discrete robust optimization algorithm for engineering design, Appl. Math. Model. 53 (2018) 602–621.
[14] J. Xiong, A. Vaziri, R. Ghosh, H. Hu, L. Ma, L. Wu, Compression behavior and energy absorption of carbon fiber reinforced composite sandwich panels made of three-dimensional honeycomb grid cores, Extreme Mech. Lett. 7 (2016) 114–120.
[15] S. Wu, G. Zheng, G. Sun, Q. Liu, G. Li, Q. Li, On design of multi-cell thin-wall structures for crashworthiness, Int. J. Impact Eng. 88 (2016) 102–117.
[16] R. Olsson, Analytical prediction of damage due to large mass impact on thin ply composites, Composites Part A Appl. Sci. Manuf. 72 (2015) 184–191.

[17] S. Seifoori, H. Hajabdollahi, Impact behavior of single-layered graphene sheets based on analytical model and molecular dynamics simulation, Appl. Surf. Sci. 351 (2015) 565–572.
[18] S. Abrate, Modeling of impacts on composite structures, Compos. Struct. 51 (2) (2001) 129–138.
[19] A. Christoforou, S. Swanson, Analysis of impact response in composite plates, Int. J. Solid Struct. 27 (2) (1991) 161–170.
[20] E. González, P. Maimí, P. Camanho, A. Turon, J. Mayugo, Simulation of drop-weight impact and compression after impact tests on composite laminates, Compos. Struct. 94 (11) (2012) 3364–3378.
[21] V. Tita, J. De Carvalho, D. Vandepitte, Failure analysis of low velocity impact on thin composite laminates: experimental and numerical approaches, Compos. Struct. 83 (4) (2008) 413–428.
[22] C. Li, N. Hu, Y. Yin, H. Sekine, H. Fukunaga, Low-velocity impact-induced damage of continuous fiber-reinforced composite laminates. Part I. An FEM numerical model, Composites Part A Appl. Sci. Manuf. 33 (8) (2002) 1055–1062.
[23] A. Ignatova, S. Sapozhnikov, N.Y. Dolganina, Development of microstructural and voxel based models of deformation and failure of the porous ceramics for assessment of ballistic performance, Int. J. Mech. Sci. 131 (2017) 672–682.
[24] K. Osnes, T. Børvik, O.S. Hopperstad, Testing and modelling of annealed float glass under quasi-static and dynamic loading, Eng. Fract. Mech. 201 (2018) 107–129.
[25] D.J. Elder, R.S. Thomson, M.Q. Nguyen, M.L. Scott, Review of delamination predictive methods for low speed impact of composite laminates, Compos. Struct. 66 (1–4) (2004) 677–683.
[26] A. Riccio, F. Caputo, G. Di Felice, S. Saputo, C. Toscano, V. Lopresto, A joint numerical-experimental study on impact induced intra-laminar and inter-laminar damage in laminated composites, Appl. Compos. Mater. 23 (3) (2016) 219–237.
[27] A. Riccio, A. Raimondo, S. Saputo, A. Sellitto, M. Battaglia, G. Petrone, A numerical study on the impact behaviour of natural fibres made honeycomb cores, Compos. Struct. 202 (2018) 909–916.
[28] B.A. Gama, J.W. Gillespie Jr., Finite element modeling of impact, damage evolution and penetration of thick-section composites, Int. J. Impact Eng. 38 (4) (2011) 181–197.
[29] Z. Hashin, Assessment of the self consistent scheme approximation: conductivity of particulate composites, J. Compos. Mater. 2 (3) (1968) 284–300.
[30] A. Gilioli, A. Manes, M. Giglio, T. Wierzbicki, Predicting ballistic impact failure of aluminium 6061-T6 with the rate-independent Bao–Wierzbicki fracture model, Int. J. Impact Eng. 76 (2015) 207–220.
[31] X. Li, X.-L. Gao, S. Kleiven, Behind helmet blunt trauma induced by ballistic impact: a computational model, Int. J. Impact Eng. 91 (2016) 56–67.
[32] R. Scazzosi, A. Manes, M. Giglio, Analytical model of high-velocity impact of a deformable projectile against textile-based composites, J. Mater. Eng. Perform. 28 (6) (2019) 3247–3255.
[33] S.G. Nunes, R. Scazzosi, A. Manes, S.C. Amico, W.F. de Amorim Júnior, M. Giglio, Influence of projectile and thickness on the ballistic behavior of aramid composites: experimental and numerical study, Int. J. Impact Eng. 132 (2019), 103307.
[34] B.A. Cheeseman, T.A. Bogetti, Ballistic impact into fabric and compliant composite laminates, Compos. Struct. 61 (1–2) (2003) 161–173.
[35] O.K. Ajibose, M. Wiercigroch, A.R. Akisanya, Experimental studies of the resultant contact forces in drillbit–rock interaction, Int. J. Mech. Sci. 91 (2015) 3–11.
[36] O.K. Ajibose, M. Wiercigroch, E. Pavlovskaia, A.R. Akisanya, Global and local dynamics of drifting oscillator for different contact force models, Int. J. Non Lin. Mech. 45 (9) (2010) 850–858.
[37] J.J. Andrew, S.M. Srinivasan, A. Arockiarajan, H.N. Dhakal, Parameters influencing the impact response of fiber-reinforced polymer matrix composite materials: a critical review, Compos. Struct. 224 (2019), 111007.
[38] J. Pach, D. Pyka, K. Jamroziak, P. Mayer, The experimental and numerical analysis of the ballistic resistance of polymer composites, Compos. B Eng. 113 (2017) 24–30.
[39] A.R. Moallemzadeh, A.R. Sabet, H. Abedini, Mechanical and morphological study of polymer composite plates having different fiber surface treatments with particular response to high velocity projectile impact, Iran. Polym. J. (Engl. Ed.) 26 (3) (2017) 229–238.
[40] A. Taherzadeh-Fard, G. Liaghat, H. Ahmadi, O. Razmkhah, S.C. Charandabi, M. A. Zarezadeh-mehrizi, A. Khodadadi, Experimental and numerical investigation of the impact response of elastomer layered fiber metal laminates (EFMLs), Compos. Struct. 245 (2020), 112264.
[41] P. Chabera, A. Boczkowska, A. Morka, T. Niezgoda, A. Ozięblo, A. Witek, Numerical and experimental study of armour system consisted of ceramic and ceramic-elastomer composites, Bull. Pol. Ac.: Tech. 62 (4) (2014).
[42] M. Sasso, G. Palmieri, G. Chiappini, D. Amodio, Characterization of hyperelastic rubber-like materials by biaxial and uniaxial stretching tests based on optical methods, Polym. Test. 27 (8) (2008) 995–1004.
[43] H. Pouriayevali, Y. Guo, V. Shim, A visco-hyperelastic constitutive description of elastomer behaviour at high strain rates, Procedia Eng 10 (2011) 2274–2279.
[44] M.R. Ahmad, W.Y.W. Ahmad, J. Salleh, A. Samsuri, Effect of fabric stitching on ballistic impact resistance of natural rubber coated fabric systems, Mater. Des. 29 (7) (2008) 1353–1358.
[45] V. Kurushina, E. Pavlovskaia, M. Wiercigroch, VIV of flexible structures in 2D uniform flow, Int. J. Eng. Sci. 150 (2020), 103211.
[46] H. Yang, X. Yao, Z. Zheng, L. Gong, L. Yuan, Y. Yuan, Y. Liu, Highly sensitive and stretchable graphene-silicone rubber composites for strain sensing, Compos. Sci. Technol. 167 (2018) 371–378.
[47] C. Roland, D. Fragiadakis, R. Gamache, Elastomer–steel laminate armor, Compos. Struct. 92 (5) (2010) 1059–1064.
[48] E. Sarlin, M. Apostol, M. Lindroos, V.-T. Kuokkala, J. Vuorinen, T. Lepistö, M. Vippola, Impact properties of novel corrosion resistant hybrid structures, Compos. Struct. 108 (2014) 886–893.
[49] M.M. Stoll, V. Sessner, M. Kramar, J. Technau, K.A. Weidenmann, The effect of an elastomer interlayer thickness variation on the mechanical properties of fiber-metal-laminates, Compos. Struct. 219 (2019) 90–96.
[50] W. Hufenbach, A. Langkamp, M. Gude, C. Ebert, A. Hornig, S. Nitschke, H. Böhm, Characterisation of strain rate dependent material properties of textile reinforced thermoplastics for crash and impact analysis, Procedia Mater. Sci. 2 (2013) 204–211.
[51] A. Khodadadi, G. Liaghat, H. Ahmadi, A.R. Bahramian, Y. Anani, O. Razmkhah, S. Asemeni, Numerical and experimental study of impact on hyperelastic rubber panels, Iran. Polym. J. (Engl. Ed.) 28 (2) (2019) 113–122.
[52] C. Wang, T. Ren, Y. Miao, T. Suo, Z. Tang, Y. Li, High-velocity impact response of CFRP panels reinforced with stiffeners, Compos. Struct. 246 (2020), 112392.
[53] A.K. Bandaru, V.V. Chavan, S. Ahmad, R. Alagirusamy, N. Bhatnagar, Ballistic impact response of Kevlar® reinforced thermoplastic composite armors, Int. J. Impact Eng. 89 (2016) 1–13.
[54] S. Ghannadpour, M. Shakeri, Application of a new energy-based collocation method for nonlinear progressive damage analysis of imperfect composite plates, Thin-Walled Struct. 147 (2020), 106369.
[55] S. Ghannadpour, M. Shakeri, A.K. Barvaj, Ultimate strength estimation of composite plates under combined in-plane and lateral pressure loads using two different numerical methods, Steel Compos. Struct. 29 (6) (2018) 785–802.
[56] A. Khodadadi, G. Liaghat, A.R. Bahramian, H. Ahmadi, Y. Anani, S. Asemani, O. Razmkhah, High velocity impact behavior of Kevlar/rubber and Kevlar/epoxy composites: a comparative study, Compos. Struct. 216 (2019) 159–167.
[57] N. Nair Shaktivesh, N. Naik, Ballistic impact behavior of 2D plain weave fabric targets with multiple layers: analytical formulation, Int. J. Damage Mech. 24 (1) (2015) 116–150.
[58] J. Harding, E. Wood, J. Campbell, Tensile testing of materials at impact rates of strain, J. Mech. Eng. Sci. 2 (2) (1960) 88–96.
[59] C. Ma, L. Freund, The Extent of the Stress Intensity Factor Field during Crack Growth under Dynamic Loading Conditions, 1986.
[60] J. Duffy, J. Campbell, R. Hawley, On the Use of a Torsional Split Hopkinson Bar to Study Rate Effects in 1100-0 Aluminum, 1971.
[61] M.M. Shokrieh, M.J. Omidi, Investigating the transverse behavior of Glass–Epoxy composites under intermediate strain rates, Compos. Struct. 93 (2) (2011) 690–696.
[62] R.W. Ogden, Nonlinear Elasticity, Anisotropy, Material Stability and Residual Stresses in Soft Tissue, Biomechanics of Soft Tissue in Cardiovascular Systems, Springer2003, pp. 65-108.
[63] J. Ruzicka, M. Spaniel, A. Prantl, J. Dzugan, J. Kuzelka, M. Moravec, Identification of ductile damage parameters in the abaqus, Bullletin of Applied Mechanics 8 (32) (2012) 89–92.
[64] J. Bencomo-Cisneros, A. Tejeda-Ochoa, J. García-Estrada, C. Herrera-Ramírez, A. Hurtado-Macías, R. Martínez-Sánchez, J. Herrera-Ramírez, Characterization of Kevlar-29 fibers by tensile tests and nanoindentation, J ALLOY COMPD 536 (2012) S456–S459.
[65] N. Kordani, A.S. Vanini, Different method to make laminates by shear thickening fluid, Sci. Eng. Compos. Mater. 21 (3) (2014) 421–425.
[66] S. Sethi, B.C. Ray, Environmental effects on fibre reinforced polymeric composites: evolving reasons and remarks on interfacial strength and stability, Adv in Colloid Interface Sci.ens. 217 (2015) 43–67.